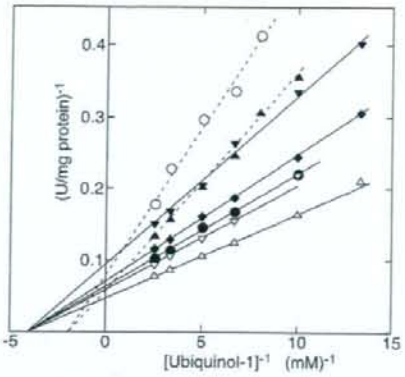

Fig. 4. Effects of antibiotics LL-Z1272 on kinetic parameters for Q_1H_2 oxidation by trypanosome AOX. Kinetic analysis was carried out in the absence of inhibitors (△) and the presence of 200 nM LL-Z1272β (▼), 20 nM LL-Z1272γ (●), 50 nM LL-Z1272δ (▲), 1 μM LL-Z1272ε (○) and 50 nM LL-Z1272ζ (▽), and 5 nM AF (◆). For clarity we showed data for one concentration of each inhibitor. The apparent K_m and V_{max} values determined for the control were 232 μM and 19.8 U/mg protein, respectively. The apparent K_i values for non-competitive inhibition by LL-Z1272β, γ, ζ, and AF were 142, 59, 203, and 2.65 nM. K_i and K_i' values for mixed-type inhibition by LL-Z1272δ and LL-Z1272ε were 0.032 and 25.5 μM and 0.483 and 9.61 μM, respectively.

and apparent K_m and V_{max} values were determined to be 232 μM and 20 U/mg protein (Fig. 4). The K_m value in 0.1% sucrose monolaurate was comparable to 350 μM for *T. b. brucei* AOX in 0.25% *n*-octyl-β-D-glucopyranoside *plus* 0.025% EDT-20 [34], but smaller than approximately 700 μM determined for *T. b. brucei* AOX in the absence of detergents [13,23]. Since the K_m value of *T. vivax* AOX for ubiquinol-2 was 116 μM (data not shown), the length of the isoprene unit may increase the binding affinity for ubiquinones [35]. The K_m of trypanosome AOX for ubiquinol-9 in *T. b. brucei* mitochondria would be comparable to the K_m value of cytochrome *bd* for ubiquinol-8 in *E. coli*.

Kinetic analysis of inhibition of *T. vivax* AOX by antibiotics LL-Z1272 revealed that LL-Z1272β (K_i=142 nM), γ (59 nM), and ζ (203 nM) act as (apparently) non-competitive inhibitors (Fig. 4), as reported for AF [13] and salicylhydroxamic acid (SHAM, K_i=25 μM) [34]. Since the amount of active AOX molecules in the *E. coli* membranes was difficult to estimate, we did not try kinetic analysis for tight-binding inhibitors [36]. In contrast, LL-Z1272δ and ε serve as mixed-type inhibitors with K_i and K_i' values of 0.032 and 25.5 μM and 0.483 and 9.61 μM, respectively.

4. Discussion

From the screening of natural antibiotics of the Kitasato Institute for Life Sciences Chemical Library, we identified prenylphenols LL-Z1272β, γ, δ, ε and ζ as a unique set of inhibitors, which can inhibit and discriminate bacterial and trypanosomal ubiquinol oxidases (Table 1). LL-Z1272β and ε (dechlorinated derivatives) inhibited cytochrome *bd*-type oxidase while LL-Z1272γ, δ, and ζ (chlorinated derivatives) were potent inhibitors of cytochrome *bo*-type oxidase and trypanosome AOX. Aurachin C is a potent inhibitor for both cytochrome *bo* and *bd* [20,27], while AF is more active against trypanosome AOX [13]. Since all three quinol oxidases are absent from mammalian mitochondria, prenylphenols could be used as lead compounds for development of novel chemotherapeutic agents [13,14,37]. However, except for the effect of LL-Z1272β on *Clostridium perfringens* (minimum inhibitory concentration of 25 μg/ml), antibiotics LL-Z1272 were ineffective against *S. aureus*, *Pseudomonas aeruginosa*, *Mycobacterium smegmatis*, and *Bacteroides fragilis*. Neither LL-Z1272γ nor LL-Z1272ε affected the aerobic growth of *E. coli* cells expressing cytochrome *bo* or *bd* as the sole terminal oxidase, likely due to the excretion by drug efflux pumps or due to the inefficient penetration through the lipopolysaccharide layer of the outer membrane.

Kinetic analysis of the inhibition of quinol oxidases by prenylphenols yielded rather complicated inhibition mechanisms (Figs. 2–4). Structural similarities of prenylphenols to ubiquinones (Fig. 1) indicate that all these compounds would act as competitive inhibitors for the quinol oxidation site. However, in many cases we found non-competitive or mixed type inhibition. In the case of tight binding inhibitors [36], Michaelis–Menten plots resemble to those of non-competitive inhibition. Alternatively, orientation of the phenol ring of prenylphenol molecules within the binding pocket will determine interactions of prenyl tails and/or the cyclohexanone ring with the protein moiety. The latter interactions would affect the former interactions. In addition, modifications of the prenyl tail (*i.e.*, the presence of the cyclohexanone or franone ring) could alter interactions with lipid bilayers and detergent micelles, which would then affect the orientation of inhibitor molecules relative to the binding pocket in quinol oxidases. Inhibition mechanisms of natural antibiotics may be inherently associated with their structural complexity, as found for inhibitors for alternative NADH dehydrogenase NDH-II [38].

Currently approved drugs for the treatment of human sleeping sickness caused by *T. b. rhodesiense* and *T. b. gambiense* are suramine, pentamidine, melarsoprol, and eflornithine [37]. They are not available for oral administration and *T. brucei* strains resistant to one or more drugs are now emerging. Thus there is an urgent need for less-toxic and more convenient new drugs against African trypanosomiasis. In parallel studies, we recently found trypanocidal activity of LL-Z1272β [39]. LL-Z1272β and LL-Z1272δ have been shown to be less toxic to human cells [18,33] and we have demonstrated that the efficacy of AF in the treatment of trypanosome-infected mice [14]. In conclusion, antibiotics LL-Z1272 are useful as probes for understanding the quinol oxidation sites of respiratory quinol oxidases and such prenylphenols are promising leading compounds for the development of new chemotherapeutic agents for African trypanosomiasis.

Acknowledgements

We thank Dr. M. Yamamoto (aRigen Pharmaceuticals. Inc., Tokyo) for AF, Dr. S. Yoshida (Institute of Physical and Chemical Research, Saitama) for piericidin A, Dr. Rokuro Masuma (Kitasato Institute for Life Sciences) for measurements of antibacterial activities of antibiotics LL-Z1272, Dr. K. Matsushita (Yamaguchi University) for his advice on enzyme assay and Dr. R. B. Gennis (University of Illinois) for the plasmid pNG2 and the *E. coli* strain GO103. This study was supported by a Grant-in-Aid for Scientific Research (20570124 to TM), Scientific Research on Priority Areas (18073004 to KK) and Creative Scientific Research (18GS0314 to KK) from the Japanese Ministry of Education, Science, Culture, Sports, and Technology.

References

[1] T.J. Foster, The *Staphylococcus aureus* "superbug", J. Clin. Invest. 114 (2004) 1693–1696.
[2] J. Travis, Reviving the antibiotic miracle? Science 264 (1994) 360–362.
[3] S. Jünneman, Cytochrome *bd* terminal oxidase, Biochim. Biophys. Acta 1321 (1997) 107–127.
[4] T. Mogi, M. Tsubaki, H. Hori, H. Miyoshi, H. Nakamura, Y. Anraku, Two terminal quinol oxidase families in *Escherichia coli*: variations on molecular machinery for dioxygen reduction, J. Biochem. Mol. Biol. Biophys. 2 (1998) 79–110.
[5] L. Cunningham, M. Pitt, H.D. Williams, The *cioAB* genes from *Pseudomonas aeruginosa* code for a novel cyanide-insensitive terminal oxidase related to the cytochrome *bd* quinol oxidases, Mol. Microbiol. 24 (1997) 579–591.
[6] S.S. Way, S. Sallustio, R.S. Magliozzo, M.B. Goldberg, Impact of either elevated or decreased levels of cytochrome *bd* expression on *Shigella flexneri* virulence, J. Bacteriol. 181 (1999) 1229–1237.

[7] S. Endley, D. McMurray, T.A. Ficht, Interruption of the *cydB* locus in *Brucella abortus* attenuates intracellular survival and virulence in the mouse model of infection, J. Bacteriol. 183 (2001) 2454–2462.
[8] A.K. Turner, L.Z. Barber, P. Wigley, S. Muhammad, M.A. Jones, M.A. Lovell, S. Hulme, P.A. Barrow, Contribution of proton-translocating proteins to the virulence of *Salmonella enterica* serovars Typhimurium, Gallinarum, and Dublin in chickens and mice, Infect. Immun. 71 (2003) 3392–3401.
[9] L. Shi, C.D. Sohaskey, B.D. Kana, S. Dawes, R.J. North, V. Mizrahi, M.L. Gennaro, Changes in energy metabolism of *Mycobacterium tuberculosis* in mouse lung and under *in vitro* conditions affecting aerobic respiration, Proc. Natl. Acad. Sci. U. S. A. 102 (2005) 15629–15634.
[10] M. Chaudhuri, R.D. Ott, G.C. Hill, Trypanosome alternative oxidase: from molecule to function, Trends Parasitol. 22 (2006) 484–491.
[11] A.L. Moore, M.S. Albury, P.G. Crichton, C. Affourtit, Function of the alternative oxidase: is it still a scavenger? Trends Plant Sci. 7 (2002) 478–481.
[12] N. Sasaki, T. Okutomi, T. Hosokawa, Y. Nawata, K. Ando, Ascofuranone, a new antibiotic from *Ascochyta viciae*, Tetrahedron Lett. 13 (1972) 2541–2544.
[13] N. Minagawa, Y. Yabu, K. Kita, K. Nagai, N. Ohta, K. Meguro, S. Sakajo, A. Yoshimoto, An antibiotic, ascofuranone, specifically inhibits respiration and in vitro growth of long slender bloodstream forms of *Trypanosoma brucei brucei*. Mol, Biochem. Parasitol. 84 (1997) 271–280.
[14] Y. Yabu, A. Yoshida, T. Suzuki, C. Nihei, K. Kawai, N. Minagawa, T. Hosokawa, K. Nagai, K. Kita, N. Ohta, The efficacy of ascofuranone in a consecutive treatment on *Trypanosoma brucei brucei* in mice, Parasitol. Int. 52 (2003) 155–164.
[15] H. Ui, A. Ishiyama, H. Sekiguchi, M. Namatame, A. Nishihara, A. Takahashi, K. Shiomi, K. Otoguro, S. Ō mura, Selective and potent *in vitro* antimalarial activities found in four microbial metabolites, J. Antibiot. 60 (2007) 220–222.
[16] S. Takamatsu, M.-C. Rho, R. Masuma, M. Hayashi, K. Komiyama, H. Tanaka, S. Omura, A novel testosterone 5a-reductase inhibitor, 8'9'-dehydroascochlorin produced by *Verticillium* sp. FO-2787, Chem. Pharm. Bull. 42 (1994) 953–956.
[17] G.A. Ellestad, R.H. Evans Jr., M.P. Kunstmann, Terpenoid metabolites from an unidentified *Fusarium* species, Tetrahedron 25 (1969) 1323–1334.
[18] S. Hayakawa, H. Minato, K. Katagiri, The ilicicolins, antibiotics from *Cylindrocladium ilicicola*, J. Antibiot. 24 (1971) 653–654.
[19] H. Minato, T. Katayama, S. Hayakawa, K. Katagiri, Identification of ilicicolins with ascochlorin and LL-Z1272, J. Antibiot. 25 (1972) 315–316.
[20] H. Miyoshi, K. Takegami, K. Sakamoto, T. Mogi, H. Iwamura, Characterization of the ubiquinol oxidation sites in cytochromes *bo* and *bd* from *Escherichia coli* using aurachin C analogues, J. Biochem. 125 (1999) 138–142.
[21] T. Mogi, S. Endo, S. Akimoto, M. Morimoto-Tadokoro, H. Miyoshi, Glutamates 99 and 107 in transmembrane helix III of subunit I of cytochrome *bd* are critical for binding of the heme b_{595}-*d* binuclear center and enzyme activity, Biochemistry 45 (2006) 15785–15792.
[22] M. Tsubaki, T. Mogi, Y. Anraku, H. Hori, Structure of heme–copper binuclear center of the cytochrome *bo* complex of *Escherichia coli*: EPR and Fourier-transform infrared spectroscopic studies, Biochemistry 32 (1993) 6065–6072.
[23] T. Suzuki, C. Nihei, Y. Yabu, T. Hashimoto, M. Suzuki, A. Yoshida, K. Nagai, T. Hosokawa, N. Minagawa, S. Suzuki, K. Kita, N. Ohta, Molecular cloning andcharacterization of *Trypanosoma vivax* alternative oxidase (AOX) gene, a target of the trypanocide ascofuranone, Parasitol. Int. 53 (2004) 235–245.
[24] T. Mogi, H. Ui, K. Shiomi, S. Ōmura, K. Kita, Gramicidin S identified as a potent inhibitor for cytochrome *bd*-type quinol oxidase, FEBS Lett. 582 (2008) 2299–2302.
[25] S. Jünemann, J.M. Wrigglesworth, Antimycin inhibition of the cytochrome *bd* complex from *Azotobacter vinelandii* indicates the presence of a branched electron transfer pathway for the oxidation of ubiquinol, FEBS Lett. 345 (1994) 198–202.
[26] K. Kita, K. Konishi, Y. Anraku, Terminal oxidases of *Escherichia coli* aerobic respiratory chain. II. Purification and properties of cytochrome b_{558}-*d* complex from cells grown with limited oxygen and evidence of branched electron-carrying systems, J. Biol. Chem. 259 (1984) 3375–3381.
[27] B. Meunier, S.A. Madgwick, E. Reil, W. Ottemeier, P.R. Rich, New inhibitors of the quinol oxidation sites of bacterial cytochromes *bo* and *bd*, Biochemistry 34 (1995) 1076–1083.
[28] Y. Matsumoto, E. Muneyuki, D. Fujita, K. Sakamoto, H. Miyoshi, M. Yoshida, T. Mogi, Kinetic mechanism of quinol oxidation by cytochrome *bd* studied with ubiquinone-2 analogs, J. Biochem. 139 (2006) 779–788.
[29] K. Kita, K. Konishi, Y. Anraku, Terminal oxidases of *Escherichia coli* aerobic respiratory chain. I. Purification and properties of cytochrome b_{562}-*o* complex from cells in the early exponential phase of aerobic growth, J. Biol. Chem. 259 (1984) 3368–3374.
[30] K. Matsushita, L. Patel, H.R. Kaback, Cytochrome *a* oxidase from *Escherichia coli*. Characterization of the enzyme and mechanism of electrochemical proton gradient generation, Biochemistry 23 (1984) 4703–4714.
[31] M. Sato-Watanabe, T. Mogi, H. Miyoshi, H. Iwamura, K. Matsushita, O. Adachi, Y. Anraku, Structure–function studies on the ubiquinol oxidation site of the cytochrome *bo* complex from *Escherichia coli* using *p*-benzoquinones and substituted phenols, J. Biol. Chem. 269 (1994) 28899–28907.
[32] T. Mogi, T. Hirano, H. Nakamura, Y. Anraku, Y. Orii, Cu_B promotes both binding and reduction of dioxygen at the heme–copper binuclear center in the *Escherichia coli bo*-type ubiquinol oxidase, FEBS Lett. 370 (1995) 259–263.
[33] M. Gutiérrez, C. Theoduloz, J. Rodríguez, M. Lolas, G. Schmeda-Hirschmann, Bioactive metabolites from the fungus *Nectria galligena*, the main apple canker agent in Chile, J. Agric. Food Chem. 53 (2005) 7701–7708.
[34] R. Ott, K. Chibale, S. Anderson, A. Chipeleme, M. Chaudhuri, A. Guerrah, N. Colowick, G.C. Hill, Novel inhibitors of the trypanosome alternative oxidase inhibit *Trypanosoma brucei brucei* growth and respiration, Acta Trop. 100 (2006) 172–184.
[35] K. Sakamoto, H. Miyoshi, M. Ohshima, K. Kuwabara, K. Kano, T. Akagi, T. Mogi, H. Iwamura, Role of isoprenyl tail of ubiquinone in reaction with respiratory enzymes: studies with bovine heart mitochondrial complex I and *Escherichia coli bo*-type ubiquinol oxidase, Biochemistry 37 (1998) 15106–15113.
[36] P.R. Rich, S.A. Madgwick, D.A. Moss, The interactions of duroquinol, DBMIB and NQNO with the chloroplast cytochrome *bf* complex, Biochim. Biophys. Acta 1058 (1991) 312–328.
[37] A.H. Fairlamb, Chemotherapy of human African trypanosomiasis: current and future prospect, Trends Parasitol. 19 (2003) 488–494.
[38] T. Mogi, K. Matsushita, H. Miyoshi, H. Ui, K. Shiomi, S. Ōmura, K. Kita, Identification of new inhibitors for alternative NADH dehydrogenase (NDH-II). FEMS Microbiol. Lett. (in press).
[39] K. Otoguro, A. Ishiyama, M. Namatame, A. Nishihara, T. Furusawa, R. Masuma, K. Shiomi, Y. Takahashi, H. Yamada, S. Omura, Selective and potent *in vitro* antitrypanosomal activities of ten microbial metabolites, J. Antibiot. 61 (2008) 372–378.

Glossary

AOX: alternatice quinol oxidase
HQNO: 2-heptyl-4-hydroxyquinoline *N*-oxide
IC_{50}: IC_{50}, the 50% inhibitory concentration
Q_1H_2: a reduced form of Q_1, ubiquinol-1

Cell Metabolism
Article

Fasting-Induced Hypothermia and Reduced Energy Production in Mice Lacking Acetyl-CoA Synthetase 2

Iori Sakakibara,[1,2] Takahiro Fujino,[3] Makoto Ishii,[2,4] Toshiya Tanaka,[1] Tatsuo Shimosawa,[5] Shinji Miura,[6] Wei Zhang,[7] Yuka Tokutake,[8] Joji Yamamoto,[2,9] Mutsumi Awano,[10] Satoshi Iwasaki,[1,2] Toshiyuki Motoike,[2,11] Masashi Okamura,[1,9] Takeshi Inagaki,[1] Kiyoshi Kita,[10] Osamu Ezaki,[6] Makoto Naito,[13] Tomoyuki Kuwaki,[7] Shigeru Chohnan,[8] Tokuo T. Yamamoto,[14] Robert E. Hammer,[12] Tatsuhiko Kodama,[1] Masashi Yanagisawa,[2,11] and Juro Sakai[1,2,*]

[1]Laboratory for Systems Biology and Medicine, Research Center for Advanced Science and Technology, University of Tokyo, Tokyo 153-8904, Japan
[2]ERATO, Japan Science and Technology Agency (JST), Tokyo 102-0075, Japan
[3]Department of Bioscience, Integrated Center for Sciences, Ehime University Graduate School of Medicine, Ehime 791-0295, Japan
[4]Department of Neurology, Weill Cornell Medical College of Cornell University, 525 East 68th Street, New York, NY 10021, USA
[5]Department of Clinical Laboratory, Faculty of Medicine, University of Tokyo, Tokyo 113-8655, Japan
[6]Nutritional Science Program, National Institute of Health and Nutrition, 1-23-1, Toyama, Shinjuku-ku, Tokyo 162-8636, Japan
[7]Departments of Molecular & Integrative Physiology and Autonomic Physiology, Graduate School of Medicine, Chiba University, Chiba, 260-8670, Japan
[8]Department of Bioresource Science, Ibaraki University College of Agriculture, 3-21-1 Chuo, Ami, Ibaraki 300-0393, Japan
[9]Division of Nephrology, Endocrinology, and Vascular Medicine, Department of Medicine, Tohoku University Graduate School of Medicine, Sendai 980-8574, Japan
[10]Department of Biomedical Chemistry, Graduate School of Medicine, University of Tokyo, Bunkyo-ku, Tokyo 113-0033, Japan
[11]Howard Hughes Medical Institute, Department of Molecular Genetics
[12]Department of Biochemistry
University of Texas Southwestern Medical Center, Dallas, TX 75390, USA
[13]Department of Cellular Function, Division of Cellular and Molecular Pathology, Niigata University Graduate School of Medical and Dental Sciences, Niigata 951-8510, Japan
[14]Center for Advanced Genome Research, Institute of Development, Aging, and Cancer, Tohoku University, Sendai 981-8555, Japan
*Correspondence: jmsakai-tky@umin.ac.jp
DOI 10.1016/j.cmet.2008.12.008

SUMMARY

Acetate is activated to acetyl-CoA by acetyl-CoA synthetase 2 (AceCS2), a mitochondrial enzyme. Here, we report that the activation of acetate by AceCS2 has a specific and unique role in thermogenesis during fasting. In the skeletal muscle of fasted *AceCS2*$^{-/-}$ mice, ATP levels were reduced by 50% compared to *AceCS2*$^{+/+}$ mice. Fasted *AceCS2*$^{-/-}$ mice were significantly hypothermic and had reduced exercise capacity. Furthermore, when fed a low-carbohydrate diet, 4-week-old weaned *AceCS2*$^{-/-}$ mice also exhibited hypothermia accompanied by sustained hypoglycemia that led to a 50% mortality. Therefore, AceCS2 plays a significant role in acetate oxidation needed to generate ATP and heat. Furthermore, *AceCS2*$^{-/-}$ mice exhibited increased oxygen consumption and reduced weight gain on a low-carbohydrate diet. Our findings demonstrate that activation of acetate by AceCS2 plays a pivotal role in thermogenesis, especially under low-glucose or ketogenic conditions, and is crucially required for survival.

INTRODUCTION

Mammals have evolved complex metabolic systems to survive extended periods of nutrient deprivation. Under a fed condition, mammals utilize glucose as the main metabolic fuel. Under ketogenic conditions such as fasting, low-carbohydrate diet feeding, and diabetes, fatty acids and ketone bodies are utilized as the main energy sources. Ketone bodies, utilized mainly in brain and also some in skeletal muscle and heart (Fukao et al., 2004), are produced in liver from acetyl-CoA released after β oxidation of fatty acids in mitochondria. Several lines of evidence report that acetate is synthesized in the liver and utilized as an alternative fuel under ketogenic conditions. For instance, acetate concentration in livers of starved rats is quite high (Murthy and Steiner, 1973). Also, formation of free acetate by the liver has been reported from studies utilizing isolated rat liver perfusion and studies using isolated hepatocytes (Leighton et al., 1989; Seufert et al., 1974; Yamashita et al., 2001). Acetate is generated following hydrolysis of acetyl-CoA by acetyl CoA hydrolase, an end product of fatty acid oxidation in rat liver peroxisomes (Leighton et al., 1989). However, it is not known whether acetate is actually utilized as an alternative fuel (substituting for glucose, fatty acids, or ketone bodies) in peripheral tissues such as skeletal muscle, heart, brown adipose tissues (BAT), or brain.

Acetyl-CoA synthetase (AceCS, EC 6.2.1.1) ligates acetate and CoA to generate acetyl-CoA. In mammals, there are two AceCSs with similar enzymatic properties: one, designated AceCS1, is a cytosolic enzyme, whereas AceCS2 is an enzyme of the mitochondrial matrix (Fujino et al., 2001; Luong et al., 2000). AceCS1 and AceCS2 are regulated posttranscriptionally by members of the sirtuin family of deacetylases, SIRT1 and SIRT3, respectively. Both SIRT1 and SIRT3 are upregulated during caloric restriction and have been implicated as mediating

the longevity-promoting effects of caloric restriction (Schwer and Verdin, 2008; Yang et al., 2007).

AceCS1 provides acetyl-CoA for the synthesis of fatty acids and cholesterol. AceCS1 is highly expressed in liver, and its transcription is regulated by sterol regulatory element-binding proteins (SREBPs), basic helix-loop-helix leucine zipper transcription factors that activate multiple genes involved in cholesterol and fatty acid metabolism (Ikeda et al., 2001; Luong et al., 2000). By contrast, AceCS2 produces acetyl-CoA for oxidation through the tricarboxylic acid cycle to produce ATP and CO_2 (Fujino et al., 2001). AceCS2 is highly expressed in BAT, heart, and skeletal muscle. Importantly, the levels of its mRNAs in BAT, heart, and skeletal muscle are robustly increased under ketogenic conditions, whereas the level of its mRNAs in liver was barely detectable (Fujino et al., 2001). The fasting-induced transcriptional activation of AceCS2 in the skeletal muscle is largely controlled by Krüppel-like factor 15 (KLF15), a member of the Krüppel-like family of transcription factors (Yamamoto et al., 2004) that regulates many genes involved in gluconeogenesis such as phosphoenolpyruvate carboxykinase (PEPCK) and amino acid-degrading enzymes required under ketogenic conditions (Gray et al., 2007; Teshigawara et al., 2005).

To examine whether acetate is utilized as a fuel under ketogenic conditions, we generated *AceCS2*-deficient mice. In this paper, we show that AceCS2 is essential for energy expenditure under ketogenic conditions.

RESULTS

Generation of *AceCS2*-Deficient Mice

To evaluate the role of AceCS2 in vivo, we generated mice lacking *AceCS2*. We constructed an insertion-type vector that disrupts exon 1 of the mouse *AceCS2* gene (Figure 1A). Two lines of mice harboring insertions in *AceCS2* were identified by Southern blotting (Figure 1B). Genotyping was performed by PCR (Figure 1C), and the absence of AceCS2 transcripts (Figure 1D) and protein (Figure 1E) was confirmed by quantitative real-time PCR (QRT-PCR) and immunoblot analysis, respectively. Wild-type (*AceCS2*$^{+/+}$), heterozygous (*AceCS2*$^{+/-}$), and homozygous (*AceCS2*$^{-/-}$) mice were born at frequencies predicted by simple Mendelian ratios. *AceCS2*$^{-/-}$ mice of both sexes were normally fertile and typical in appearance. No histological abnormalities were seen following light microscopy of sections obtained from multiple tissues of adult male mice, including bone, brain, stomach, heart, intestine, kidney, liver, pancreas, white adipose tissue, BAT, and skeletal muscle (data not shown). At birth, the body weight and length of *AceCS2*$^{-/-}$ mice were indistinguishable from their littermates. By the time of weaning (4 weeks of age), both male and female *AceCS2*$^{-/-}$ mice exhibited significant growth retardation (Figures S1A–S1C available online). After weaning, *AceCS2*$^{-/-}$ mice fed on normal chow diet began to catch up with *AceCS2*$^{+/+}$ mice in both body weight and body length. By 20 weeks of age, the body weight of the *AceCS2*$^{-/-}$ mice became comparable to their littermates (Figures S1A and S1B). Food intake of 4-week-old *AceCS2*$^{-/-}$ mice was slightly decreased compared to *AceCS2*$^{+/+}$ mice but became comparable to that of their littermates by 20 weeks of age (Figure S1D). Plasma parameters of *AceCS2*$^{+/+}$ and *AceCS2*$^{-/-}$ mice before weaning (2–4 weeks of age) and at 26 weeks of age are shown in Table S1. Glucose, ketone bodies, nonesterified fatty acids (NEFA), and insulin levels were indistinguishable between *AceCS2*$^{+/+}$ and *AceCS2*$^{-/-}$ mice at both 2–4 weeks of age and at 26 weeks of age (Table S1). Plasma concentration of growth hormone and

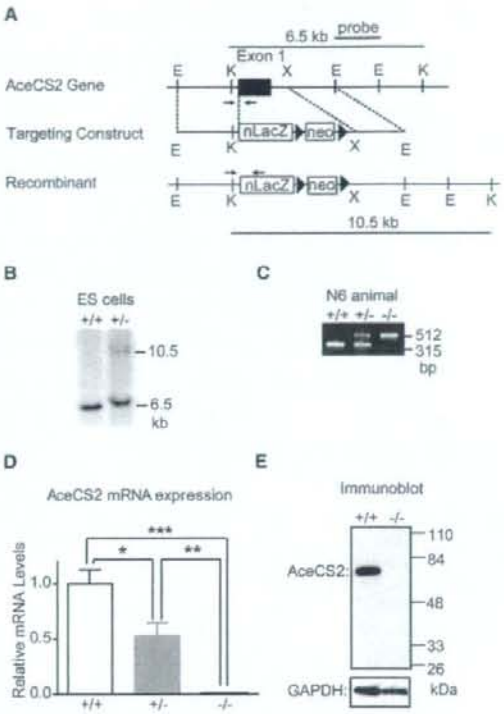

Figure 1. Generation of *AceCS2*-Deficient Mice

(A) Diagram of the targeting strategy. Only the relevant restriction sites are indicated. Locations of the probes for Southern blot analysis (bars) and PCR primers (arrows) for genotyping are shown.

(B) Southern blot analysis of KpnI-digested DNA from ES cell clones. Southern blotting was performed with the probe indicated in (A). KpnI digestion resulted in a 6.5 kb fragment in wild-type DNA and a 10.5 kb fragment in homologous recombinants.

(C) An ethidium bromide-stained agarose gel illustrates PCR products for genotyping *AceCS2*$^{+/+}$, *AceCS2*$^{+/-}$, and *AceCS2*$^{-/-}$ mice. A description of the PCR genotyping strategy is contained in the Experimental Procedures.

(D) QRT-PCR analysis of AceCS2 transcripts. Total RNA from heart of *AceCS2*$^{+/+}$, *AceCS2*$^{+/-}$, and *AceCS2*$^{-/-}$ mice were analyzed by QRT-PCR quantification as described in the Experimental Procedures. β-actin was used as the invariant control. Values represent the amount of mRNA relative to that in *AceCS2*$^{+/+}$ mice, which is arbitrarily defined as 1. Data are mean ± SEM. $^{*}p < 0.05$ compared to *AceCS2*$^{+/+}$; $^{**}p < 0.01$ compared to *AceCS2*$^{+/-}$; $^{***}p < 0.001$ compared to *AceCS2*$^{+/+}$ ($^{+/+}$, n = 9; $^{+/-}$, n = 17; $^{-/-}$, n = 7).

(E) Immunoblot analysis, with an affinity-purified anti-rabbit polyclonal AceCS2 antibody, of *AceCS2*$^{+/+}$ and *AceCS2*$^{-/-}$ mouse heart protein. Each lane was loaded with 20 μg of whole-cell lysates in SDS lysis buffer from the hearts. GAPDH was detected with a polyclonal anti-GAPDH antibody as a loading control.

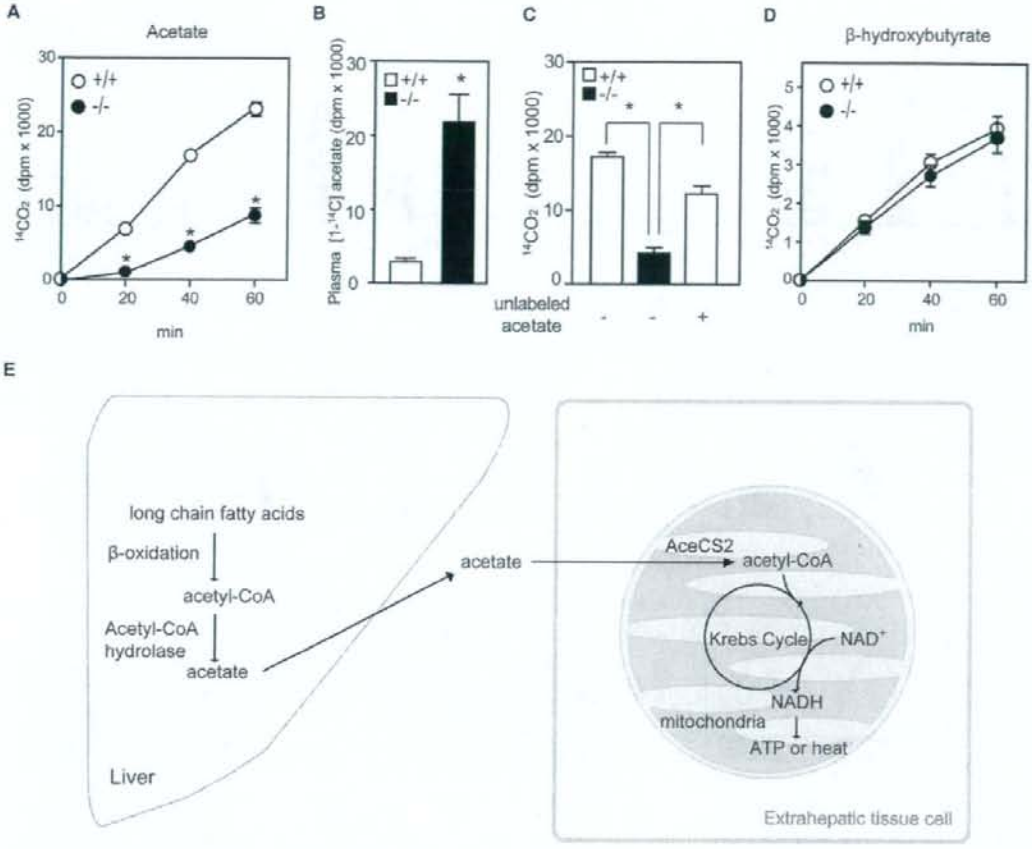

Figure 2. *AceCS2*$^{-/-}$ Mice Exhibit Lower Whole-Body Acetic Acid Oxidation during Fasting

After 48 hr of fasting, 12-week-old male mice were tested for their ability to oxidize [1-^{14}C]acetate or [1-^{14}C]β-hydroxybutyrate to $^{14}CO_2$ at 20, 40, and 60 min after intraperitoneal (i.p.) injection with the labeled compound.

(A) Rate of $^{14}CO_2$ production from acetate. *$p < 0.001$ compared to *AceCS2*$^{+/+}$.

(B) Total plasma [1-^{14}C]acetate was measured after 60 min.

(C) Rate of $^{14}CO_2$ production from acetate with inclusion of unlabeled acetate. Unlabeled acetate (0.6 g/kg) was injected with [1-^{14}C]acetate, and the acetate oxidation rate was measured after 40 min.

(D) Rate of $^{14}CO_2$ production from β-hydroxybutyrate (*AceCS2*$^{+/+}$, n = 6; *AceCS2*$^{-/-}$, n = 6).

(E) Model for the role of AceCS2 in energy metabolism.

(A–D) Data are mean ± SEM.

insulin-like growth factor-1 (IGF-1) of *AceCS2*$^{-/-}$ mice (2–4 weeks of age) were also comparable to *AceCS2*$^{+/+}$. The plasma leptin levels of 2- to 4-week-old *AceCS2*$^{-/-}$ mice were lower than those of age-matched, wild-type littermates. Notably, plasma acetate levels were markedly elevated in *AceCS2*$^{-/-}$ mice compared to *AceCS2*$^{+/+}$ mice (Table S1).

AceCS2$^{-/-}$ Mice Exhibited Marked Reduction in Whole-Body Acetate Oxidation

To examine whether acetate is, in fact, utilized as a fuel during fasting, we performed whole-body acetate oxidization assays. Mice were fasted for 48 hr and then injected with [^{14}C]acetate. Figure 2A shows the sharply decreased rate of acetate oxidation in *AceCS2*$^{-/-}$ mice. As a consequence, [^{14}C]acetate levels remained high in the plasma of *AceCS2*$^{-/-}$ mice, whereas *AceCS2*$^{+/+}$ mice showed very low levels of plasma [^{14}C]acetate (Figure 2B). Because higher levels of plasma acetate in *AceCS2*$^{-/-}$ mice might affect the acetate oxidation rate, we also examined the oxidation of [^{14}C]acetate with the inclusion of unlabeled acetate at similar levels to those found in the *AceCS2*$^{-/-}$ mice (about 2 mM) (Figure 2C). Injection of unlabeled acetate (0.6 mg/kg) led to rapid increase in plasma acetate to

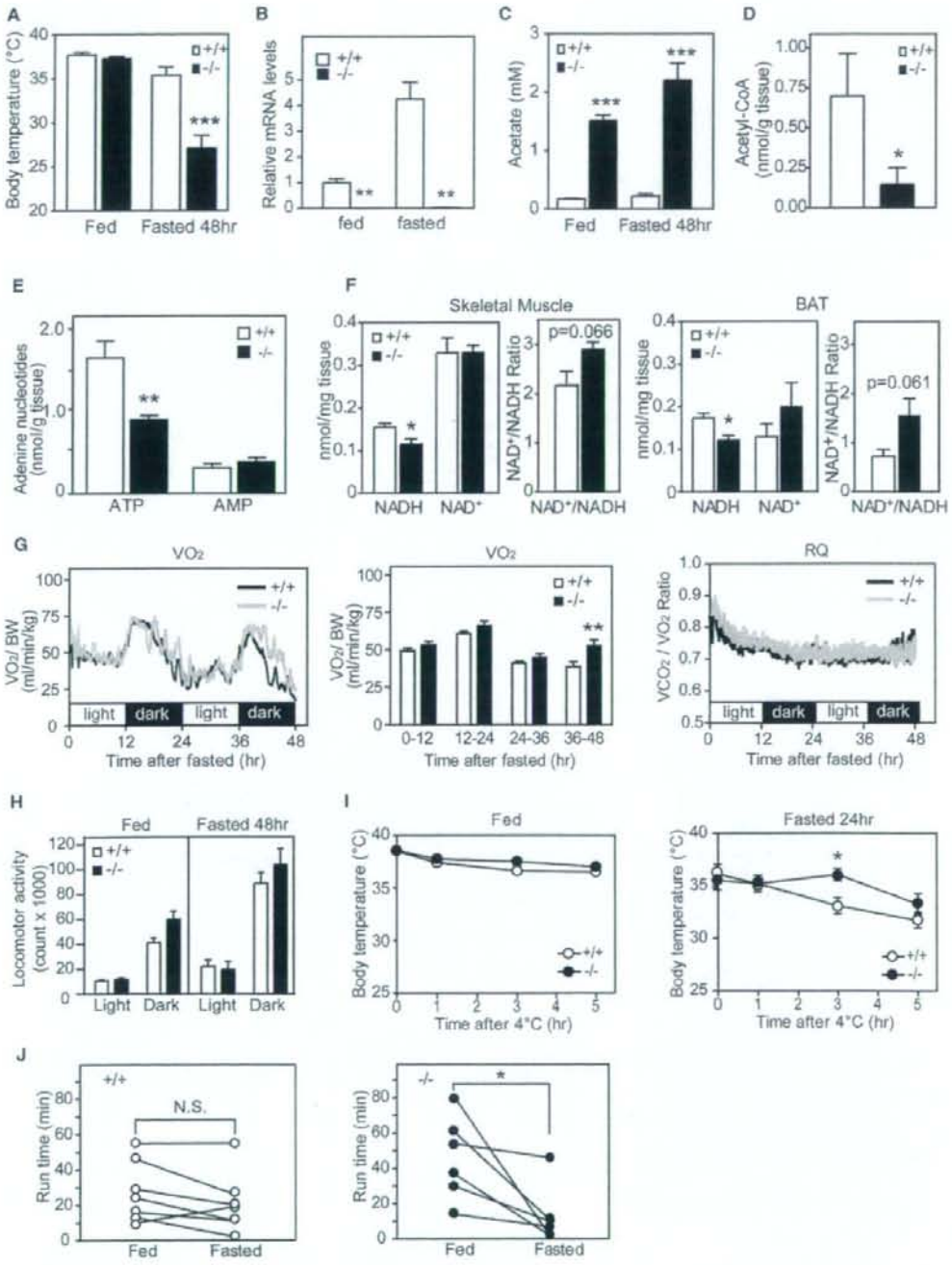
A
Body temperature (°C)
Fed
Fasted 48hr
+/+
-/-
***
B
Relative mRNA levels
fed
fasted
**
C
Acetate (mM)
***
D
Acetyl-CoA (nmol/g tissue)
*
E
Adenine nucleotides (nmol/g tissue)
ATP
AMP
**
F
Skeletal Muscle
BAT
nmol/mg tissue
NADH
NAD+
NAD+/NADH Ratio
p=0.066
p=0.061
G
VO2
VO2/ BW (ml/min/kg)
light
dark
Time after fasted (hr)
RQ
VCO2 / VO2 Ratio
0-12
12-24
24-36
36-48
H
Locomotor activity (count x 1000)
Light
Dark
I
Body temperature (°C)
Time after 4°C (hr)
Fasted 24hr
J
Run time (min)
N.S.
Fed
Fasted

2 mM at 40 min after the injection (data not shown). Under this condition, the rate of acetate oxidation measured was still significantly lower in *AceCS2*$^{-/-}$ mice (Figure 2C). Oxidation of ketone bodies was similar, irrespective of genotype (Figure 2D), indicating that ketone body utilization is normal in *AceCS2*$^{-/-}$ mice.

Together with our previous report showing that [^{14}C]acetate is incorporated into CO_2 in AceCS2-transfected cells (Fujino et al., 2001), these data indicate that, in mice, acetate oxidation to form CO_2 and ATP requires AceCS2. Previous studies showed that an appreciable amount of acetate is generated in liver by hepatic acetyl-CoA hydrolase, a ubiquitous peroxisome enzyme, and that this acetate can subsequently be utilized by extrahepatic tissues (Leighton et al., 1989; Murthy and Steiner, 1973; Seufert et al., 1974). We propose a model in which acetate is generated in liver from fatty acids and released into the circulation under conditions when glucose is low, such as 48 hr fasting or low-carbohydrate/ high-fat diet. AceCS2 is necessary for salvaging this acetate for use in extrahepatic tissues such as skeletal muscle and BAT, where acetate is reactivated for reentry to the mitochondrial TCA cycle to generate ATP and heat (Figure 2E).

Adult *AceCS2*$^{-/-}$ Mice Exhibit Low Body Temperature and Reduced Capacity to Sustain Running Exercise under a Fasting Condition

To further evaluate the physiological role of acetate oxidation, 12-week-old *AceCS2*$^{-/-}$ mice were freely fed a standard rodent diet or fasted for 48 hr. During normal fed states, there was no significant difference in core temperature between *AceCS2*$^{+/+}$ and *AceCS2*$^{-/-}$ mice (Figure 3A). After 48 hr of fasting, *AceCS2*$^{+/+}$ mice were able to maintain their core body temperatures, but *AceCS2*$^{-/-}$ mice had significantly lower core body temperatures (Figure 3A). These data demonstrate that acetate activation by AceCS2 is important for maintenance of normal body temperature, likely as a result of heat production during fasting. Indeed, the mRNA levels in BAT of AceCS2 were 4-fold higher under the fasted condition than under the fed condition, suggesting that AceCS2 has an important role during fasting condition (Figure 3B).

In mice, BAT and skeletal muscle are the main thermogenic tissues in which oxidation of fatty acid, stimulated by the sympathetic nervous system, generates heat through uncoupling proteins (UCPs) present in mitochondria (Spiegelman and Flier, 2001). During fasting, the quantity and morphology of mitochondria in BAT and skeletal muscle are indistinguishable between *AceCS2*$^{+/+}$ mice and sex- and age-matched *AceCS2*$^{-/-}$ mice (Figure S2A). Oxidative proteins such as UCPs are thought to be important in thermogenesis (Matthias et al., 2000; Spiegelman and Flier, 2001). The mRNA levels of UCP1 in the BAT or UCP2 and UCP3 in the skeletal muscle did not differ significantly between *AceCS2*$^{+/+}$ and *AceCS2*$^{-/-}$ mice. Other thermogenic molecules PGC1α and PPARδ also did not differ in mRNA levels (Figure S2B and data not shown).

To evaluate substrate supply, we determined the levels of various metabolites in the plasma of fed and 48 hr fasted 12-week-old male *AceCS2*$^{+/+}$ and *AceCS2*$^{-/-}$ mice (Table S2). There was no significant change in plasma glucose or in NEFA and ketone body levels between *AceCS2*$^{+/+}$ and *AceCS2*$^{-/-}$ mice (Table S2). There was also no significant difference in the percentage of fat mass between fed *AceCS2*$^{-/-}$ and *AceCS2*$^{+/+}$ mice as assessed by dual-energy X-ray absorption (DEXA) (Table S2). However, plasma acetate was 5- to 10-fold higher in *AceCS2*$^{-/-}$ mice as compared to *AceCS2*$^{+/+}$ mice under both fed and fasted conditions (Figure 3C). These data indicate that acetate utilization is impaired in *AceCS2*$^{-/-}$ mice, implying that a deficit in extrahepatic acetate utilization causes fasting-induced hypothermia. Acetyl-CoA levels were decreased by 75% in fasted *AceCS2*$^{-/-}$ mice (Figure 3D). NADH and ATP levels in skeletal muscles of fasted *AceCS2*$^{-/-}$ mice were significantly reduced compared to those found in *AceCS2*$^{+/+}$ mice (Figures 3E and 3F). These data indicate that AceCS2 plays a pivotal role in supplying acetyl-CoA for ATP production during 48 hr of fasting. Oxygen consumption was significantly increased after 36 hr fasting, and locomotor activity was not reduced (Figures 3G and 3H).

The hypothermia in *AceCS2*$^{-/-}$ mice also differs from adaptive hypothermia in response to cold (Lowell and Spiegelman, 2000). Exposure of these *AceCS2*$^{-/-}$ mice to low temperature (4°C) did

Figure 3. *AceCS2*-Deficient Mice Exhibit Low Body Temperature and Reduced Exercise Capacity during Fasting

(A) Core temperature of male mice (12 weeks old) fed on normal chow diet was monitored after 48 hr fasting (*AceCS2*$^{+/+}$, n = 8; *AceCS2*$^{-/-}$, n = 7). *$p < 0.05$ compared to *AceCS2*$^{+/+}$.

(B) Relative mRNA expression levels of AceCS2 in BAT of male mice (12 weeks old, six to seven per genotype). **$p < 0.01$ compared to *AceCS2*$^{+/+}$.

(C) Plasma acetate levels of male mice (12 weeks old) fed or fasted for 48 hr (fed *AceCS2*$^{+/+}$, n = 4; fasted *AceCS2*$^{+/+}$, n = 4; fed *AceCS2*$^{-/-}$, n = 4; fasted *AceCS2*$^{-/-}$, n = 4).

(D) Acetyl-CoA levels in gastrocnemius muscle from 48 hr fasted male *AceCS2*$^{+/+}$ and *AceCS2*$^{-/-}$ mice (12 weeks old) were measured (*AceCS2*$^{+/+}$, n = 7; *AceCS2*$^{-/-}$, n = 8).

(E) ATP content is markedly reduced in *AceCS2*$^{-/-}$ mice. ATP and AMP contents of gastrocnemius muscle from male *AceCS2*$^{+/+}$ and *AceCS2*$^{-/-}$ mice were measured at 12 weeks of age (*AceCS2*$^{+/+}$, n = 7; *AceCS2*$^{-/-}$, n = 8). **$p < 0.01$ compared to *AceCS2*$^{+/+}$.

(F) NAD$^+$ and NADH levels and NAD$^+$/NADH ratio in gastrocnemius muscle and BAT of 48 hr fasted male *AceCS2*$^{+/+}$ and *AceCS2*$^{-/-}$ mice (12 weeks old) (*AceCS2*$^{+/+}$, n = 4; *AceCS2*$^{-/-}$, n = 4).

(G) Oxygen consumption (VO_2) (left panel), average of VO_2 (center panel), and RQ (respiratory quotient) (right panel) were determined in fasted male mice (12 weeks old) by indirect calorimetry (*AceCS2*$^{+/+}$, n = 6; *AceCS2*$^{-/-}$, n = 5).

(H) Total locomotor activity of male mice (14 weeks old) was measured by beam breaks in the light and dark periods (*AceCS2*$^{+/+}$, n = 12; *AceCS2*$^{-/-}$, n = 12).

(I) Male mice (12 weeks old) given food and water ad libitum were subjected to cold (4°C) (left panel) (*AceCS2*$^{+/+}$, n = 10; *AceCS2*$^{-/-}$, n = 11). Male mice (12 weeks old) fasted for 24 hr and given water ad libitum were subjected to cold (4°C) (right panel) (*AceCS2*$^{+/+}$, n = 7; *AceCS2*$^{-/-}$, n = 8). Core temperature was monitored over a 5 hr period.

(J) Male mice (12 weeks old, nine per genotype) were subjected to a run-to-exhaustion protocol on a motorized treadmill under fed conditions and 48 hr fasted conditions (*AceCS2*$^{+/+}$, n = 9; *AceCS2*$^{-/-}$, n = 9). *$p < 0.05$ compared to fed.

All values are mean ± SEM.

not further reduce their body temperatures under the fed condition (Figure 3I, left panel). We next examined the effect of cold exposure on 24 hr fasted mice. Unlike with 48 hr fasting, under 24 hr fasting conditions, *AceCS2*$^{-/-}$ mice maintained their core body temperatures at levels similar to *AceCS2*$^{+/+}$ mice, although both levels were equally reduced by 2°C–3°C compared to fed levels. Exposure of these mice to cold further decreased their core temperatures; however, after 5 hr cold exposure, there was no significant difference between *AceCS2*$^{-/-}$ and *AceCS2*$^{+/+}$ mice (Figure 3I, right panel). These data indicate that adaptive thermogenesis in response to low temperature was not impaired in *AceCS2*$^{-/-}$ mice and further suggest that the sympathetic nervous system is able to properly maintain core body temperature in *AceCS2*$^{-/-}$ mice.

We hypothesized that fasting *AceCS2*$^{-/-}$ mice would lead to decreased exercise tolerance, owing to impaired acetate oxidation and subsequent reduction of ATP production in skeletal muscle (Figure 3E). *AceCS2*$^{-/-}$ mice were exercised on a motorized treadmill apparatus using a run-to-exhaustion protocol. *AceCS2*$^{-/-}$ mice fasted for 48 hr exhibited a markedly reduced capacity to sustain running exercise, whereas the running capacity of *AceCS2*$^{+/+}$ mice did not change between the fed and fasted conditions (Figure 3J). This suggests that acetate is an important fuel required for exercise as well as for heat generation during fasting.

AceCS2$^{-/-}$ Mice Compensate for Metabolic Acidosis through Hyperventilation

Because the plasma acetate levels are very high in *AceCS2*$^{-/-}$ mice, we speculated that these mice could be acidotic, and, if not, they might be hyperventilating to blow off CO_2 to prevent acidemia. Accordingly, we measured the arterial blood gases, pH, and bicarbonate concentration. The values of arterial carbon dioxide partial pressure ($PaCO_2$) were significantly decreased in *AceCS2*$^{-/-}$ mice ($p < 0.05$, $n = 5–6$), indicating that *AceCS2*$^{-/-}$ mice were hyperventilating to blow off CO_2. There were no significant differences in the values of PaO_2, standardized bicarbonate concentration ($[HCO_3^-]$), and the pH (Table 1). These data indicate that *AceCS2*$^{-/-}$ mice were hyperventilating to compensate for a possible acidosis caused by acetate accumulation. This hyperventilation in *AceCS2*$^{-/-}$ mice might account for some of their increased energy expenditure compared to *AceCS2*$^{+/+}$ mice.

AceCS2$^{-/-}$ Mice Exhibit Hypothermia and Hypoglycemia under Low-Carbohydrate, High-Fat Diet

Similar to fasting conditions, we hypothesized that acetate utilization may be important under low-glucose or low-carbohydrate intake states. To examine this possibility, 4-week-old *AceCS2*$^{-/-}$ and *AceCS2*$^{+/+}$ mice were fed a low-carbohydrate, high-fat diet (LC/HF; 0.4% carbohydrate, 90.5% fat, and 9.1% protein from calories). At the time of weaning (4 weeks of age), *AceCS2*$^{-/-}$ mice weighed an average of 40% less than their littermates (Figures S1A–S1C), and plasma acetate levels were markedly elevated (Figure 4A). Plasma ketone bodies, NEFA, glucose, and insulin levels were comparable between *AceCS2*$^{+/+}$ and *AceCS2*$^{-/-}$ mice (Table S1).

On LC/HF diet, *AceCS2*$^{-/-}$ mice exhibited lower body temperatures (Figure 4B). This was most severe (30.1 ± 1.4°C) on day 2 of LC/HF diet feeding, whereas *AceCS2*$^{+/+}$ mice maintained their body temperatures at 37°C on this diet. In addition, *AceCS2*$^{-/-}$ mice lost weight, whereas the body weight of *AceCS2*$^{+/+}$ mice remained stable (Figure 4C). Furthermore, *AceCS2*$^{-/-}$ mice had sustained hypoglycemia (56 ± 5 mg/dl) over this period compared to *AceCS2*$^{+/+}$ mice that exhibited transiently decreased plasma glucose levels at weaning but soon recovered to normal levels (137 ± 7 mg/dl) (Figure 4D). This transient hypoglycemia in *AceCS2*$^{+/+}$ is most likely from the stress of forced weaning, which causes suppression of feeding on the day of weaning. Plasma NEFA and ketone body levels were highly elevated, but there were no significant differences between *AceCS2*$^{+/+}$ and *AceCS2*$^{-/-}$ mice except in ketone body levels on day 3 of the LC/HF diet (Figures 4E and 4F). The abundance of mRNAs for the enzymes involved in gluconeogenesis was not decreased in *AceCS2*$^{-/-}$ mice compared to *AceCS2*$^{+/+}$ mice (Figure S3A). Furthermore, injection of pyruvate to these mice rescued hypoglycemia (Figure S3B), indicating that the gluconeogenic pathway is intact.

Table 1. Blood Gas Analysis of *AceCS2*$^{+/+}$ and *AceCS2*$^{-/-}$ Mice

	+/+	−/−
pH	7.34 ± 0.03	7.34 ± 0.03
PaO_2 (mm Hg)	102.3 ± 2.7	108.8 ± 5.5
$PaCO_2$ (mm Hg)	37.3 ± 1.2	33.3 ± 0.9[a]
HCO_3^- (mM)	19.7 ± 0.8	17.6 ± 1.3
BE (mM)	−5.1 ± 1.2	−6.9 ± 1.9

Male mice (12 weeks old, n = 6 per genotype) were fed on a normal chow diet. Samples were obtained from the femoral artery of awake, freely moving mice. Data are mean ± SEM.
[a] $p < 0.05$ compared to *AceCS2*$^{+/+}$.

After 5 days of LC/HF diet feeding, *AceCS2*$^{-/-}$ mice began to die, and, by 21 days, 50% of the *AceCS2*$^{-/-}$ mice had died. By contrast, none of *AceCS2*$^{+/+}$ mice died (Figure 4G). However, following 21 days on the LC/HF diet, the surviving *AceCS2*$^{-/-}$ mice gradually recovered body temperature and plasma glucose levels. We observed no further excess mortality (data not shown).

Weight, body temperature, and plasma parameters (glucose, NEFA, and ketone bodies) did not differ significantly between the *AceCS2*$^{-/-}$ mice that died and those that survived during the 4 day period of LC/HF feeding after the weaning (Figures S4A–S4E). Therefore, the cause of death was not simply from malnutrition. We also examined the effect of a high-carbohydrate, high-fat (HC/HF) diet (58% fat, 15% protein, and 27% carbohydrate from calories). On this diet, both *AceCS2*$^{-/-}$ and *AceCS2*$^{+/+}$ mice survived with no deaths (data not shown). These data indicated that acetate oxidation mediated by AceCS2 is essential to maintain normal thermogenesis and fuel usage under low-glucose utilization states such as low-carbohydrate diets or fasting.

AceCS2$^{-/-}$ Mice Exhibit Low Body Weight Gain under Low Carbohydrate Intake

We continued to feed the surviving *AceCS2*$^{-/-}$ mice an LC/HF diet. *AceCS2*$^{+/+}$ mice fed on this diet gained weight efficiently; by contrast, *AceCS2*$^{-/-}$ mice exhibited reduced weight gain under this diet (Figure 5A). Food intake was unchanged between

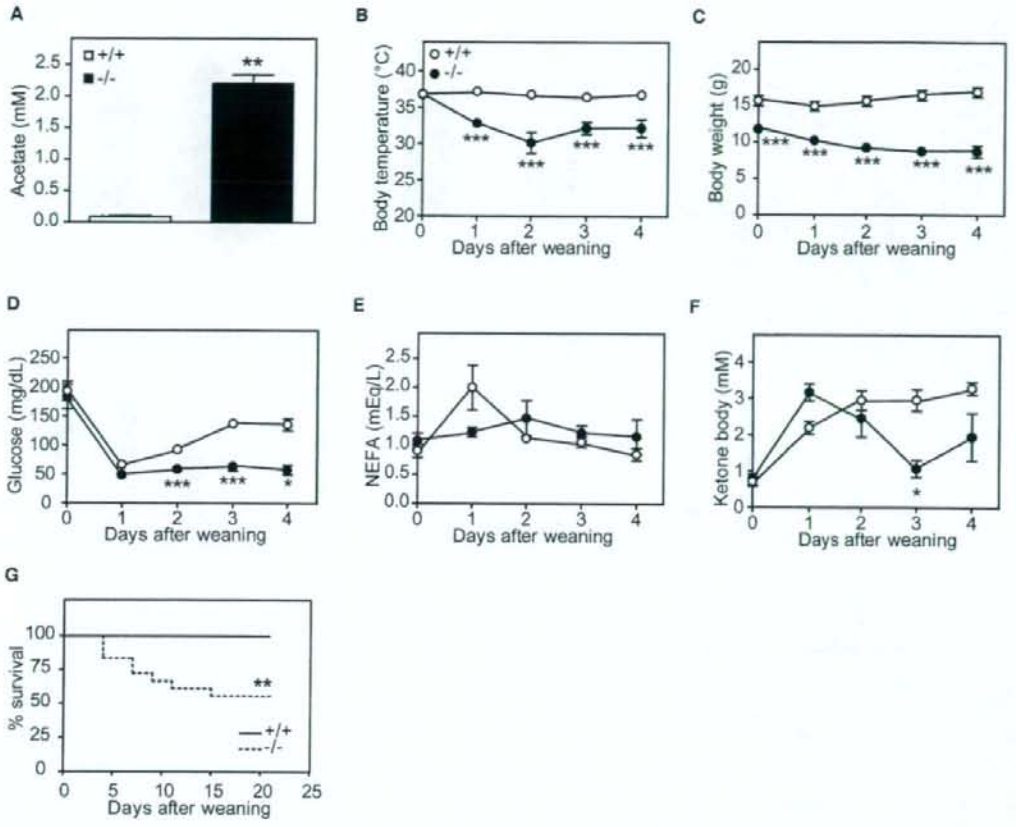

Figure 4. *AceCS2*-Deficient Mice Exhibit Hypothermia When Fed an LC/HF Diet

(A) Male mice (4 weeks old, five per genotype) were fed milk from their mother. Plasma acetate levels were measured.

(B–F) Male mice (4 weeks old) were fed an LC/HF diet. (B) Core rectal temperature, (C) body weight, (D) blood glucose, (E) plasma NEFA, and (F) plasma ketone body level were measured (*AceCS2*$^{+/+}$, n = 8; *AceCS2*$^{-/-}$, n = 7). *p < 0.05, **p < 0.01, and ***p < 0.001 compared to *AceCS2*$^{+/+}$.

(G) Kaplan-Meier analysis of survival in males fed an LC/HF diet at 4 weeks old (*AceCS2*$^{+/+}$, n = 22; *AceCS2*$^{-/-}$, n = 18). **p < 0.001 compared to *AceCS2*$^{+/+}$ by Log-rank test. Data are mean ± SEM.

AceCS2$^{+/+}$ and *AceCS2*$^{-/-}$ mice (Figure 5B). We excised various tissues from these mice and measured tissue weights. The photo shown in Figure 5C was taken for representative mice of each group. There were no marked differences in the weights of liver, kidney, BAT, and heart between *AceCS2*$^{+/+}$ and *AceCS2*$^{-/-}$ mice, but the fat pads of *AceCS2*$^{-/-}$ mice were significantly smaller than those of *AceCS2*$^{+/+}$ mice (Figure 5D). We measured metabolic parameters of these mice at 24 weeks of age (Table 2). Although the plasma glucose levels were unchanged, plasma insulin levels decreased significantly in *AceCS2*$^{-/-}$ mice as compared to *AceCS2*$^{+/+}$ mice. Plasma levels of leptin were 4-fold lower, but plasma acetate was 7-fold higher in *AceCS2*$^{-/-}$ mice (Table 2).

In order to investigate the mechanism underlying reduced weight gain in *AceCS2*$^{-/-}$ mice, food intake and energy expenditure were examined. *AceCS2*$^{-/-}$ mice exhibited consistently higher rates of oxygen consumption and, therefore, had higher metabolic rates than *AceCS2*$^{+/+}$ mice throughout day and night (Figure 5E). After adjusting for allometric scaling and gender, the effect of the *AceCS2*$^{-/-}$ allele was highly significant ($p < 0.01$, n = 7, multiple ANOVA) (Figure 5E, right panel). The respiratory quotient was 0.71 in both *AceCS2*$^{+/+}$ and *AceCS2*$^{-/-}$ mice (data not shown). These data suggested that the resistance to weight gain of *AceCS2*$^{-/-}$ mice may be, at least in part, due to increased energy expenditure. To examine the possibility that fatty acids synthesis is changed in *AceCS2*$^{-/-}$ mice, we measured malonyl-CoA levels and acetyl-CoA carboxylase (ACC) activity (Figure S5). Malonyl-CoA levels and ACC activity in skeletal muscle and BAT did not significantly differ between *AceCS2*$^{-/-}$ and *AceCS2*$^{+/+}$ mice (Figure S5). In liver, malonyl-CoA levels

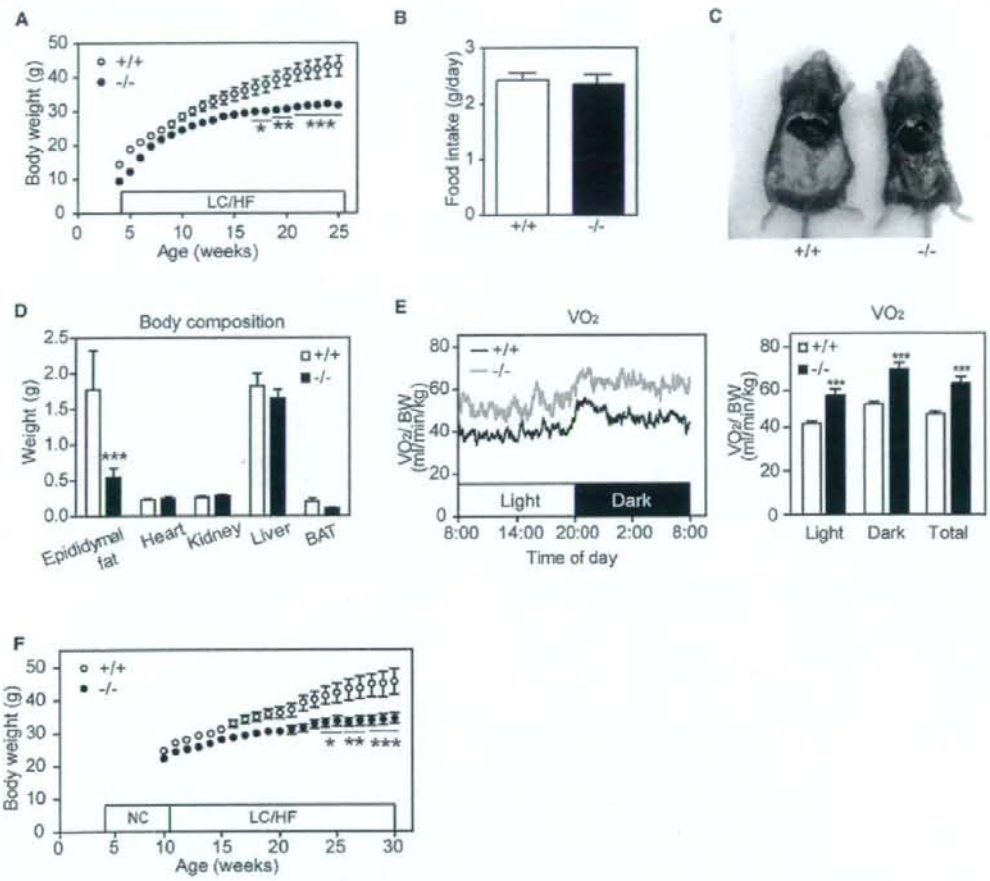

Figure 5. *AceCS2* Deficiency Attenuates Body Weight Gain in Mice Fed an LC/HF Diet

(A) Body weight change of male mice fed an LC/HF diet from 4 weeks old (*AceCS2*$^{+/+}$, n = 15; *AceCS2*$^{-/-}$, n = 12).

(B) Food intake of male mice fed an LC/HF diet at 25 weeks old (*AceCS2*$^{+/+}$, n = 15; *AceCS2*$^{-/-}$, n = 12).

(C) Representative picture of *AceCS2*$^{+/+}$ and *AceCS2*$^{-/-}$ male mice (26 weeks of age) fed an LC/HF diet.

(D) Various tissue weights for *AceCS2*$^{+/+}$ and *AceCS2*$^{-/-}$ male mice (26 weeks of age) fed an LC/HF diet (*AceCS* $^{+/+}$, n = 5; *AceCS2*$^{-/-}$, n = 5).

(E) Oxygen consumption (VO_2, left panel) and average of VO_2 (right panel) were determined in male mice (26 weeks old) fed an LC/HF diet by indirect calorimetry (*AceCS2*$^{+/+}$, n = 8; *AceCS2*$^{-/-}$, n = 7). Data are corrected for body weight. The original, uncorrected data are shown in Figure S6.

(F) Change of body weight. Male mice were weaned at 4 weeks and were fed on normal chow diet for 6 weeks (until 10 weeks of age) and switched to an LC/HF diet (*AceCS2*$^{+/+}$, n = 8; *AceCS2*$^{-/-}$, n = 8). *$p < 0.05$, **$p < 0.01$, and ***$p < 0.001$ compared to *AceCS2*$^{+/+}$. Data are mean ± SEM. NC, normal chow diet.

were reduced by 20% in *AceCS2*$^{-/-}$ (Figure S5), which could be the secondary effect of lower plasma insulin levels since AceCS2 is not expressed in liver. These data suggested that fatty acid synthesis and degradation are not impaired by the deficiency of *AceCS2*.

It is possible that the reduced weight gain of *AceCS2*$^{-/-}$ mice during LC/HF diet feeding simply resulted from a failure to thrive phenotype (reduced body weight gain, hypothermia, hypoglycemia, and low survival rate) induced by low-carbohydrate diet feeding immediately after weaning (Figure 4). Therefore, after weaning, we first fed the mice a normal chow diet for 6 weeks (until 10 weeks of age) and then switched them to an LC/HF diet. By contrast to feeding an LC/HF diet immediately after weaning, none of these *AceCS2*$^{-/-}$ mice died; however, they did exhibit reduced weight gain compared to *AceCS2*$^{+/+}$ mice following the switch to an LC/HF diet (Figure 5F). Reduced weight gain was observed only under a low-carbohydrate regimen. When mice were fed a high-fat, high-carbohydrate diet, *AceCS2*$^{-/-}$ mice were not protected against weight gain (data not shown). These results clearly indicate that adult

Table 2. Metabolic Parameters of *AceCS2*$^{-/-}$ and *AceCS2*$^{+/+}$ Mice Fed an LC/HF Diet

	+/+	−/−
Glucose (mg/dl)	233 ± 14	233 ± 22
Cholesterol (mg/dl)	110 ± 7	70 ± 11[b]
Triglycerides (mg/dl)	93 ± 6	92 ± 9
NEFA (μEq/l)	343 ± 17	332 ± 71
Ketone body (mM)	0.387 ± 0.064	0.705 ± 0.116[a]
Leptin (ng/ml)	2.80 ± 1.12	0.74 ± 1.03[b]
Insulin (ng/ml)	3.34 ± 1.3	1.54 ± 0.71[a]
Acetate (mM)	0.18 ± 0.06	0.97 ± 0.17[b]

Male mice (24 weeks old, seven to nine per genotype) were fed an LC/HF diet. Assays of blood samples were performed on isolated plasma.
[a] $p < 0.05$.
[b] $p < 0.01$ compared to *AceCS2*$^{+/+}$.

AceCS2$^{-/-}$ mice exhibit reduced adiposity under high-fat feeding, low-carbohydrate intake, or ketogenic conditions.

DISCUSSION

Under ketogenic conditions, free fatty acids are released into the circulation and taken up by thermogenic tissues such as BAT and skeletal muscle, where they serve as a fuel for thermogenesis (Picard et al., 2002; Spiegelman and Flier, 2001). Fatty acids are also taken up by liver for the generation of ketone bodies, and these ketone bodies are subsequently utilized in extrahepatic tissues. In addition, previous studies showed that an appreciable amount of acetate is generated in liver and this acetate can subsequently be utilized by extrahepatic tissues (Leighton et al., 1989; Murthy and Steiner, 1973; Seufert et al., 1974). Here, we demonstrate that acetate also serves as a fuel that has specific functions that do not overlap with those of fatty acids and ketone bodies in thermogenesis.

Our studies of mice with targeted deletion of *AceCS2* reveal that these animals can not maintain normal body temperature when starved or when fed an LC/HF diet. Under these conditions, *AceCS2*$^{-/-}$ mice display sustained hypoglycemia, strongly diminished capacity for exercise, and dramatically increased mortality as compared to their wild-type or heterozygous littermates. The mutant animals also exhibit strikingly reduced rates of whole-body acetate oxidation and correspondingly increased levels of acetate in plasma. Most importantly, ATP levels in the skeletal muscle of 48 hr fasted *AceCS2*$^{-/-}$ mice were profoundly reduced, showing the significant contribution of acetate and AceCS2 to the energy supply under ketogenic conditions. Therefore, under ketogenic conditions, the hypothermia and poor exercise tolerance observed in the *AceCS2*$^{-/-}$ mice is most likely from a lack of acetate utilization as a fuel source. Supporting this possibility, plasma acetate levels were significantly higher under fasting conditions than under fed conditions. This suggests that acetate turnover is significantly higher in the fasted state primarily due to AceCS2.

LC/HF diet has been generally recognized to have weight-reducing effects on obese animals (Kennedy et al., 2007). Although the body weight gain of mice fed an LC/HF diet is significantly lower than that of those fed high-fat and high-carbohydrate diets, our LC/HF diet has no weight-reducing or anti-weight-gaining effect. In the experiments done by Kennedy et al. (2007), 8-week-old mice fed a normal chow diet were switched to an LC/HF diet, and the weight of mice fed an LC/HF diet dropped until it stabilized at 85% of the initial weight. The discrepancy between these results may result from the difference in the composition of the different LC/HF diets. The LC/HF diet that Kennedy et al. used consists of 78.85% fat, 9.5% protein, and 0.76% carbohydrate, whereas our LC/HF diet (purchased from Harlan Teklad) contains 67.4% fat, 15.3% protein, and 0.6% carbohydrate (% by weight). In addition, the source of the fat is also different. The LC/HF diet in their study contains lard and butter, whereas our LC/HF diet contains vegetable shortening. Regardless of the differences in the exact diet, we show that AceCS2 is critical for normal body weight gain under an LC/HF diet.

Recent observations indirectly support a role for *AceCS2* as a determinant of growth and adiposity. From the mapping of a quantitative trait locus (QTL) region on mouse chromosome 2 that has a large effect on growth and adiposity, AceCS2 was reported as 1 of 18 candidate genes potentially controlling predisposition to growth and predisposition to obesity (Jerez-Timaure et al., 2005).

Although plasma acetate is very high in *AceCS2*$^{-/-}$ mice, we found that there was appropriate and sufficient respiratory compensation for any metabolic acidosis caused by acetate accumulation. *AceCS2*$^{-/-}$ mice exhibited hypocapnea to maintain a neutral arterial blood pH. Patients with chronic obstructive lung disease and cystic fibrosis commonly have low body weight, which is believed to be related to inadequate energy intake, nutrient malabsorption, and excessive energy expenditure (Bell et al., 1996). Basal metabolic rate is 10%–20% greater in these patients than in healthy subjects and may contribute to their energy imbalance. Furthermore, increased oxygen consumption caused by increased respiratory muscle activity has been reported in these patients, which largely explains the increased basal metabolic rate (Campbell et al., 1959; Cherniack, 1959; Donahoe et al., 1989; McGregor and Becklake, 1961). Because *AceCS2*$^{-/-}$ mice seem to be hyperventilating, this increased use of respiratory muscles might account for, at least in part, the higher oxygen consumption.

We previously identified AceCS2 as a target of KLF15 (Yamamoto et al., 2004). The fasting-induced transcription of AceCS2 is largely dependent on KLF15. Similarly to *AceCS2*$^{-/-}$ mice, KLF15-deficient mice also exhibit severe hypoglycemia after overnight fasting (Fisch et al., 2007). KLF15 plays an important role in gluconeogenesis by regulating amino acid degradation and key gluconeogenic enzymes such as phosphoenolpyruvate carboxykinase in the liver during fasting (Gray et al., 2007; Teshigawara et al., 2005). Our data indicate that KLF15 is crucial for survival during starvation through two mechanisms: (1) gluconeogenesis in liver and (2) acetate oxidation to generate ATP and heat in muscle and BAT through AceCS2 activity.

The sirtuins comprise a conserved family of proteins that are believed to mediate some of the health benefits of calorie restriction, which leads to extension of life span in nearly all organisms studied, including mammals. SIRT1 has been reported to function as an energy-sensing gene that senses NAD^+ levels and regulates the activity of critical transcriptional regulators of

metabolism in multiple tissues (Yang et al., 2007). Within the mitochondria, SIRT3 deacetylates a key lysine residue on AceCS2, leading to its enzymatic activation (Hallows et al., 2006; Schwer et al., 2006; Schwer and Verdin, 2008). As SIRT3 protein levels are specifically increased in calorie-restricted mammals, regulation of AceCS2 activity by SIRT3 could be a key metabolic factor responsible for homeostatic regulation during calorie restriction, leading to its positive effect on life span. Sirt3 was recently shown to be necessary for maintaining basal ATP levels with ATP levels in multiple organs of *Sirt3*$^{-/-}$ mice that are markedly reduced compared to wild-type levels (Ahn et al., 2008). This study, along with ours, suggests that activation of AceCS2 by Sirt3 is required to maintain basal ATP levels in mammals. Future studies of AceCS2- and AceCS2-deficient mice are warranted to investigate this potentially exciting link between longevity and mitochondrial energy metabolism.

In conclusion, our current findings demonstrate that acetate metabolism mediated by AceCS2 is crucial for survival and energy production under ketogenic conditions such as starvation or diabetes. These and future studies of acetate metabolism mediated by AceCS2 will have a significant impact on the understanding of the acetate metabolism for heat generation and energy metabolism.

EXPERIMENTAL PROCEDURES

Generation of AceCS2-Deficient Mice

We constructed a targeting plasmid by using genomic DNA fragments derived from Sv129 mice. A Lac Z and a neomycin cassette flanked by two loxP sites were introduced into the *AceCS2* locus of ES cells (derived from the Sv129 strain). Electroporation, selection, and screening were performed with standard gene-targeting techniques. Briefly, genomic DNA was isolated from neomycin-resistant ES cell clones, digested with KpnI, and subjected to hybridization with a probe to detect homologous recombination and the presence of the flox allele (Figure 1A).

Chimeric males were generated by using the morula aggregation technique and mated to C57BL/6J female mice. Homologous recombination was confirmed by Southern blotting (Figure 1B). Deletion of RNA transcripts and protein was confirmed by QRT-PCR and western blotting, respectively (Figures 1D and 1E). After achieving germline transmission, *AceCS2*$^{+/-}$ mice were crossed with C57BL/6J for six to nine generations.

Heterozygous mice were mated to obtain *AceCS2*$^{-/-}$ mice. Wild-type littermates were used as controls throughout the study. Genotyping of mice used in this study was performed by PCR of tail DNA as shown in Figure 1C; the mutant allele was detected by using a pair of oligonucleotides (5′-GGCGCACAACAAAACCTAGT-3′ and 5′-GACAGTATCGGCCTCAGGAA-3′) that amplify a 512 bp PCR product between the *AceCS2* and sequence 3′ to *Lac Z/neo* cassette. The wild-type allele was detected by PCR with a pair of oligonucleotides (5′-GGCGCACAACAAAACCTAGT-3′ and 5′-GGGGTTCGTGCCTGGTTG-3′) that amplify a 355 bp PCR product spanning exon 1.

Quantitative Real-Time PCR

Quantitative real-time PCR (QRT-PCR) was performed as previously described (Tanaka et al., 2003). All primer sequences used in this paper are available upon request.

Antibody

To produce rabbit polyclonal anti-murine AceCS2 (IgGA001), a 12-residue peptide corresponding to the C terminus of murine AceCS2 (CQKYEEQ RAATN) was synthesized (Sigma Genesis, Japan), coupled to keyhole limpet hemocyanin, and injected into New Zealand White rabbits. IgG fractions were prepared by affinity chromatography on protein A-Sepharose (GE Healthcare Bioscience). For immunoblot analysis, an aliquot of whole-cell lysates from heart (20 μg) was subjected to SDS-PAGE on 10% gels followed by analysis with a 1:1000 dilution of anti-AceCS2 (Fujino et al., 2001).

Animal Experiments

All procedures were performed in accordance with Japanese Physiological Society guidelines for animal care. Mice were group housed in cages with a 12 hr light/12 hr dark cycle and fed a standard rodent chow diet (CE-2; CLEA Japan, Osaka). To induce a ketogenic condition, we compared an LC/HF diet (Table S3; Rho et al., 1999) (TD96355; Harlan Teklad Premier Laboratory Diets) consisting of 90.5% fat, 9.1% protein, and 0.4% carbohydrate (0% sucrose from calories) to a high-carbohydrate, high-fat diet consisting of 58.0% fat, 15.0% protein, and 27.01% carbohydrate from calories (Tanaka et al., 2003). All mice had free access to water. Food consumption was monitored daily, and body weight was recorded every week, unless otherwise stated.

Core body temperature was monitored using a rectal thermometer at 10 a.m. For the exercise performance, the mice were trained on the treadmill (MK-680AT/02M, Muromachikikai, Tokyo) prior to the exercise performance test (a 10 min run at 10 m/min at a 5° incline once per day for 4 days). Exhaustion was defined as the point at which mice were unable to continue running.

Food Intake, Locomotor Activity, and Metabolic Rate Measurement

Male mice (26 weeks old) were housed under controlled lighting (12 hr light-dark cycle) and temperature (23°C) conditions. Food (standard chow pellets or an LC/HF diet) and water were available ad libitum. Mice were then housed singly under the same conditions as above for an acclimation period of at least 7 days. Body weights and food intake were monitored daily for the duration of the study. Energy expenditure was measured by indirect calorimetry as described previously (MK-5000RQ; Muromachi, Tokyo) (Takayasu et al., 2006). Mice were placed in the calorimeter chambers and acclimated for 1 day. Locomotor activity was measured by using an infrared (IR) passive sensor system as described previously (Supermex, Muromachi Kikai, Japan) (Takayasu et al., 2006). The experiment was started at 8 a.m. (light period).

Acetate Oxidation

Acetate ([1-^{14}C]acetate, CFA13, GE Healthcare UK Limited) oxidation was measured in vivo as described (Wolfgang et al., 2006). The in vivo rate of ^{14}C-acetate oxidation (2 μCi [1 Ci = 37 GBq] of [1-^{14}C]acetate injected intraperitoneally) to $^{14}CO_2$ was determined after treatment of mice. Mice were acclimated in metabolic chambers fitted with 2-aminoethanol traps to recover expired $^{14}CO_2$. The oxidation of [1-^{14}C]acetate to form $^{14}CO_2$ was measured at 20 min intervals over the next 1 hr. At the end of experiment, plasma was collected, and plasma [1-^{14}C]acetate was measured.

Acetate Measurement

Plasma acetate levels were measured as described by (Hillman et al. 1978) with slight modifications. Briefly, plasma was mixed with 1 mM isovaleric acid as the internal standard. The sample was acidified with one-fifth the volume of 10% sulfosalicylic acid and then extracted three times with 10 volumes of diethylether. The ether extract was immediately back extracted into 0.2 M NaOH. The ether was removed under a stream of dry nitrogen. Before injection, the sample was reacidified with one-fifth the volume of 10% phosphoric acid. The acetate concentration of the sample was analyzed by gas chromatograph (GC-2014, Shimadzu, Japan) equipped with a flame ionization detector and a capillary column (ULBON HR-20 M, 0.25 mm i.d. × 25 m × 0.25 μm). The column was operated at 140°C. The injection port and the flame ionization detector were maintained at 300°C. The chromatograph was standardized with a mixture of C2-C7 short-chain fatty acids.

Plasma Parameters

Mice were sacrificed by CO_2 asphyxiation following a 4 hr fast during the light cycle (food removed 9:00 a.m., sacrificed at 1:00 p.m.). Blood was drawn by cardiac puncture, and the plasma was separated immediately by centrifugation and stored at −80°C until use. Plasma glucose, NEFA, triglycerides, total cholesterol, and total ketone body levels were determined by Glucose C2-test (Wako Pure Chemical, Japan), NEFA C-test (Wako Pure Chemical, Japan), Triglyceride E-test (Wako Pure Chemical, Japan), Cholesterol E-test (Wako Pure Chemical, Japan), and Autokit Total Ketone Bodies (Wako Pure

Chemical, Japan), respectively. Plasma insulin and leptin levels were determined by ELISA with an insulin immunoassay kit (Shibayagi, Japan) and a mouse leptin immunoassay (R & D systems) according to the manufacturer's instructions.

Assay Procedure for Acetyl-CoA, Adenine Nucleotides, NAD$^+$, and NADH Contents

Acetyl-CoA and adenine nucleotide contents in skeletal muscle or BAT of 12-week-old male mice were measured essentially as described previously (Miura et al., 2006; Scott et al., 1992; Takamura et al., 1985). NAD$^+$ and NADH nucleotide concentrations were directly measured by NAD$^+$/NADH Assay kit (Biochain Institute, Inc.) according to the manufacturer's instructions. The detail methods are described in the Supplemental Experimental Procedures.

Blood Gas Analysis

Blood gas analysis was performed as previously described (Kuwaki et al., 1996). A catheter was implanted into the right femoral artery under isoflurane (2%–3%) anesthesia. Up to 70 μl of arterial blood was drawn from the indwelling catheter after a recovery period of more than 2 hr and when the animal was quietly awake. Blood gases were determined by a blood gas analyzer (ABL500, Radiometer, Copenhagen).

Statistical Analyses

All values are expressed as mean ± standard error of the mean unless otherwise specified. Significant differences between mean values were evaluated using two-tailed, unpaired Student's t test (when two groups were analyzed) or one-way ANOVA followed by Student Newman-Keuls test (for three or more groups).

SUPPLEMENTAL DATA

Supplemental Data include Supplemental Experimental Procedures, six figures, and three tables and can be found with this article online at: http://www.cell.com/cell-metabolism/supplemental/S1550-4131(08)00393-8.

ACKNOWLEDGMENTS

We thank Dr. Rob Rawson for critical reading of the manuscript; Drs. Peter Edwards and Mitsuhiro Watanabe for helpful discussions; and Kaori Ikeda, Junko Kuno, Satomi Takahashi, Yuko Kai, and Mika Nomiyama for technical assistance. This work was supported through ERATO JST, NIBIO by the NFAT project of the NEDO and by the Special Coordination Fund for Science and Technology from the Ministry of Education, Culture, Sports, Science, and Technology. This work was also supported, in part, by Astellas Foundation for Research on Metabolic Disorders, the Uehara Memorial Foundation, and the Ono Medical Foundation. M.Y. is an Investigator of the Howard Hughes Medical Institute. J.S. is an Investigator of Translational Systems Biology and Medicine Initiative (TSBMI).

Received: June 6, 2008
Revised: October 15, 2008
Accepted: December 12, 2008
Published: February 3, 2009

REFERENCES

Ahn, B.H., Kim, H.S., Song, S., Lee, I.H., Liu, J., Vassilopoulos, A., Deng, C.X., and Finkel, T. (2008). A role for the mitochondrial deacetylase Sirt3 in regulating energy homeostasis. Proc. Natl. Acad. Sci. USA *105*, 14447–14452.

Bell, S.C., Saunders, M.J., Elborn, J.S., and Shale, D.J. (1996). Resting energy expenditure and oxygen cost of breathing in patients with cystic fibrosis. Thorax *51*, 126–131.

Campbell, E.J., Westlake, E.K., and Cherniack, R.M. (1959). The oxygen consumption and efficiency of the respiratory muscles of young male subjects. Clin. Sci. (Lond.) *18*, 55–64.

Cherniack, R.M. (1959). The oxygen consumption and efficiency of the respiratory muscles in health and emphysema. J. Clin. Invest. *38*, 494–499.

Donahoe, M., Rogers, R.M., Wilson, D.O., and Pennock, B.E. (1989). Oxygen consumption of the respiratory muscles in normal and in malnourished patients with chronic obstructive pulmonary disease. Am. Rev. Respir. Dis. *140*, 385–391.

Fisch, S., Gray, S., Heymans, S., Haldar, S.M., Wang, B., Pfister, O., Cui, L., Kumar, A., Lin, Z., Sen-Banerjee, S., et al. (2007). Kruppel-like factor 15 is a regulator of cardiomyocyte hypertrophy. Proc. Natl. Acad. Sci. USA *104*, 7074–7079.

Fujino, T., Kondo, J., Ishikawa, M., Morikawa, K., and Yamamoto, T.T. (2001). Acetyl-CoA synthetase 2, a mitochondrial matrix enzyme involved in the oxidation of acetate. J. Biol. Chem. *276*, 11420–11426.

Fukao, T., Lopaschuk, G.D., and Mitchell, G.A. (2004). Pathways and control of ketone body metabolism: On the fringe of lipid biochemistry. Prostaglandins Leukot. Essent. Fatty Acids *70*, 243–251.

Gray, S., Wang, B., Orihuela, Y., Hong, E.G., Fisch, S., Haldar, S., Cline, G.W., Kim, J.K., Peroni, O.D., Kahn, B.B., et al. (2007). Regulation of gluconeogenesis by Kruppel-like factor 15. Cell Metab. *5*, 305–312.

Hallows, W.C., Lee, S., and Denu, J.M. (2006). Sirtuins deacetylate and activate mammalian acetyl-CoA synthetases. Proc. Natl. Acad. Sci. USA *103*, 10230–10235.

Hillman, R.E. (1978). Simple, rapid method for determination of propionic acid and other short-chain fatty acids in serum. Clin. Chem. *24*, 800–803.

Ikeda, Y., Yamamoto, J., Okamura, M., Fujino, T., Takahashi, S., Takeuchi, K., Osborne, T.F., Yamamoto, T.T., Ito, S., and Sakai, J. (2001). Transcriptional regulation of the murine acetyl-CoA synthetase 1 gene through multiple clustered binding sites for sterol regulatory element-binding proteins and a single neighboring site for Sp1. J. Biol. Chem. *276*, 34259–34269.

Jerez-Timaure, N.C., Eisen, E.J., and Pomp, D. (2005). Fine mapping of a QTL region with large effects on growth and fatness on mouse chromosome 2. Physiol. Genomics *21*, 411–422.

Kennedy, A.R., Pissios, P., Otu, H., Xue, B., Asakura, K., Furukawa, N., Marino, F.E., Liu, F.F., Kahn, B.B., Libermann, T.A., et al. (2007). A high-fat, ketogenic diet induces a unique metabolic state in mice. Am. J. Physiol. Endocrinol. Metab. *292*, E1724–E1739.

Kuwaki, T., Cao, W.H., Kurihara, Y., Kurihara, H., Ling, G.Y., Onodera, M., Ju, K.H., Yazaki, Y., and Kumada, M. (1996). Impaired ventilatory responses to hypoxia and hypercapnia in mutant mice deficient in endothelin-1. Am. J. Physiol. *270*, R1279–R1286.

Leighton, F., Bergseth, S., Rortveit, T., Christiansen, E.N., and Bremer, J. (1989). Free acetate production by rat hepatocytes during peroxisomal fatty acid and dicarboxylic acid oxidation. J. Biol. Chem. *264*, 10347–10350.

Lowell, B.B., and Spiegelman, B.M. (2000). Towards a molecular understanding of adaptive thermogenesis. Nature *404*, 652–660.

Luong, A., Hannah, V.C., Brown, M.S., and Goldstein, J.L. (2000). Molecular characterization of human acetyl-CoA synthetase, an enzyme regulated by sterol regulatory element-binding proteins. J. Biol. Chem. *275*, 26458–26466.

Matthias, A., Ohlson, K.B., Fredriksson, J.M., Jacobsson, A., Nedergaard, J., and Cannon, B. (2000). Thermogenic responses in brown fat cells are fully UCP1-dependent. UCP2 or UCP3 do not substitute for UCP1 in adrenergically or fatty scid-induced thermogenesis. J. Biol. Chem. *275*, 25073–25081.

McGregor, M., and Becklake, M.R. (1961). The relationship of oxygen cost of breathing to respiratory mechanical work and respiratory force. J. Clin. Invest. *40*, 971–980.

Miura, S., Tomitsuka, E., Kamei, Y., Yamazaki, T., Kai, Y., Tamura, M., Kita, K., Nishino, I., and Ezaki, O. (2006). Overexpression of peroxisome proliferator-activated receptor gamma co-activator-1alpha leads to muscle atrophy with depletion of ATP. Am. J. Pathol. *169*, 1129–1139.

Murthy, V.K., and Steiner, G. (1973). Hepatic acetate levels in relation to altered lipid metabolism. Metabolism *22*, 81–84.

Picard, F., Gehin, M., Annicotte, J., Rocchi, S., Champy, M.F., O'Malley, B.W., Chambon, P., and Auwerx, J. (2002). SRC-1 and TIF2 control energy balance between white and brown adipose tissues. Cell *111*, 931–941.

Rho, J.M., Kim, D.W., Robbins, C.A., Anderson, G.D., and Schwartzkroin, P.A. (1999). Age-dependent differences in flurothyl seizure sensitivity in mice treated with a ketogenic diet. Epilepsy Res. *37*, 233–240.

Schwer, B., Bunkenborg, J., Verdin, R.O., Andersen, J.S., and Verdin, E. (2006). Reversible lysine acetylation controls the activity of the mitochondrial enzyme acetyl-CoA synthetase 2. Proc. Natl. Acad. Sci. USA *103*, 10224–10229.

Schwer, B., and Verdin, E. (2008). Conserved metabolic regulatory functions of sirtuins. Cell Metab. *7*, 104–112.

Scott, M.D., Baudendistel, L.J., and Dahms, T.E. (1992). Rapid separation of creatine, phosphocreatine and adenosine metabolites by ion-pair reversed-phase high-performance liquid chromatography in plasma and cardiac tissue. J. Chromatogr. *576*, 149–154.

Seufert, C.D., Graf, M., Janson, G., Kuhn, A., and Soling, H.D. (1974). Formation of free acetate by isolated perfused livers from normal, starved and diabetic rats. Biochem. Biophys. Res. Commun. *57*, 901–909.

Spiegelman, B.M., and Flier, J.S. (2001). Obesity and the regulation of energy balance. Cell *104*, 531–543.

Takamura, Y., Kitayama, Y., Arakawa, A., Yamanaka, S., Tosaki, M., and Ogawa, Y. (1985). Malonyl-CoA: Acetyl-CoA cycling. A new micromethod for determination of acyl-CoAs with malonate decarboxylase. Biochim. Biophys. Acta *834*, 1–7.

Takayasu, S., Sakurai, T., Iwasaki, S., Teranishi, H., Yamanaka, A., Williams, S.C., Iguchi, H., Kawasawa, Y.I., Ikeda, Y., Sakakibara, I., et al. (2006). A neuropeptide ligand of the G protein-coupled receptor GPR103 regulates feeding, behavioral arousal, and blood pressure in mice. Proc. Natl. Acad. Sci. USA *103*, 7438–7443.

Tanaka, T., Yamamoto, J., Iwasaki, S., Asaba, H., Hamura, H., Ikeda, Y., Watanabe, M., Magoori, K., Ioka, R.X., Tachibana, K., et al. (2003). Activation of peroxisome proliferator-activated receptor delta induces fatty acid beta-oxidation in skeletal muscle and attenuates metabolic syndrome. Proc. Natl. Acad. Sci. USA *100*, 15924–15929.

Teshigawara, K., Ogawa, W., Mori, T., Matsuki, Y., Watanabe, E., Hiramatsu, R., Inoue, H., Miyake, K., Sakaue, H., and Kasuga, M. (2005). Role of Kruppel-like factor 15 in PEPCK gene expression in the liver. Biochem. Biophys. Res. Commun. *327*, 920–926.

Wolfgang, M.J., Kurama, T., Dai, Y., Suwa, A., Asaumi, M., Matsumoto, S., Cha, S.H., Shimokawa, T., and Lane, M.D. (2006). The brain-specific carnitine palmitoyltransferase-1c regulates energy homeostasis. Proc. Natl. Acad. Sci. USA *103*, 7282–7287.

Yamamoto, J., Ikeda, Y., Iguchi, H., Fujino, T., Tanaka, T., Asaba, H., Iwasaki, S., Ioka, R.X., Kaneko, I.W., Magoori, K., et al. (2004). A Kruppel-like factor KLF15 contributes fasting-induced transcriptional activation of mitochondrial acetyl-CoA synthetase gene AceCS2. J. Biol. Chem. *279*, 16954–16962.

Yamashita, H., Kaneyuki, T., and Tagawa, K. (2001). Production of acetate in the liver and its utilization in peripheral tissues. Biochim. Biophys. Acta *1532*, 79–87.

Yang, H., Yang, T., Baur, J.A., Perez, E., Matsui, T., Carmona, J.J., Lamming, D.W., Souza-Pinto, N.C., Bohr, V.A., Rosenzweig, A., et al. (2007). Nutrient-sensitive mitochondrial NAD+ levels dictate cell survival. Cell *130*, 1095–1107.

THE JOURNAL OF BIOLOGICAL CHEMISTRY VOL. 284, NO. 11, pp. 7255–7263, March 13, 2009

Novel Mitochondrial Complex II Isolated from *Trypanosoma cruzi* Is Composed of 12 Peptides Including a Heterodimeric Ip Subunit*[S]

Received for publication, August 26, 2008, and in revised form, January 2, 2009 Published, JBC Papers in Press, January 2, 2009, DOI 10.1074/jbc.M806623200

Jorge Morales[‡1], Tatsushi Mogi[‡2], Shigeru Mineki[§], Eizo Takashima[‡3], Reiko Mineki[¶], Hiroko Hirawake[‡], Kimitoshi Sakamoto[‡], Satoshi Ōmura[‖], and Kiyoshi Kita[‡4]

From the [‡]Department of Biomedical Chemistry, Graduate School of Medicine, the University of Tokyo, Hongo, Bunkyo-ku, Tokyo 113-0033, the [§]Department of Applied Biological Science, Faculty of Science and Technology, Tokyo University of Science, Noda, Chiba 278-8510, the [¶]Division of Proteomics and BioMolecular Science, Juntendo University Graduate School of Medicine, Hongo, Bunkyo-ku, Tokyo 113-8421, and the [‖]Kitasato Institute for Life Sciences and Graduate School of Infection Control Sciences, Kitasato University, Minato-ku, Tokyo 108-8641, Japan

Mitochondrial respiratory enzymes play a central role in energy production in aerobic organisms. They differentiated from the α-proteobacteria-derived ancestors by adding non-catalytic subunits. An exception is Complex II (succinate: ubiquinone reductase), which is composed of four α-proteobacteria-derived catalytic subunits (SDH1–SDH4). Complex II often plays a pivotal role in adaptation of parasites in host organisms and would be a potential target for new drugs. We purified Complex II from the parasitic protist *Trypanosoma cruzi* and obtained the unexpected result that it consists of six hydrophilic (SDH1, $SDH2_N$, $SDH2_C$, and SDH5–SDH7) and six hydrophobic (SDH3, SDH4, and SDH8–SDH11) nucleus-encoded subunits. Orthologous genes for each subunit were identified in *Trypanosoma brucei* and *Leishmania major*. Notably, the iron-sulfur subunit was heterodimeric; $SDH2_N$ and $SDH2_C$ contain the plant-type ferredoxin domain in the N-terminal half and the bacterial ferredoxin domain in the C-terminal half, respectively. Catalytic subunits (SDH1, $SDH2_N$ plus $SDH2_C$, SDH3, and SDH4) contain all key residues for binding of dicarboxylates and quinones, but the enzyme showed the lower affinity for both substrates and inhibitors than mammalian enzymes. In addition, the enzyme binds protoheme IX, but SDH3 lacks a ligand histidine. These unusual features are unique in the Trypanosomatida and make their Complex II a target for new chemotherapeutic agents.

The parasitic protist *Trypanosoma cruzi* is the etiological agent of Chagas disease, a public health threat in Central and South America. These parasites are normally transmitted by reduviid bugs via the vector feces after a bug bite and also via transfusion of infected blood. About 16–18 million people are infected, and 100 million are at risk, but there are no definitive chemotherapeutic treatments available (1). Despite having potential pathways for oxidative phosphorylation (2), all trypanosomatids (*Trypanosoma* and *Leishmania* species) analyzed so far are characterized by incomplete oxidation of glucose with secretion of end products, such as succinate, alanine, ethanol, acetate, pyruvate, and glycerol (3, 4) (Fig. 1). Major routes for formation of succinate in *Trypanosoma brucei* are via NADH-dependent fumarate reductase in glycosomes and mitochondria (5, 6). In trypanosomatid mitochondria, the Krebs cycle is inefficient, and pyruvate is principally converted to acetate via acetate:succinate CoA transferase (7). A part of the Krebs cycle operates the utilization of histidine in the insect stage of *T. cruzi* (8).

Mitochondrial Complex II (succinate:quinone reductase (SQR)[5] and succinate dehydrogenase (SDH)) serves as a membrane-bound Krebs cycle enzyme and often plays a pivotal role in adaptation of parasites to environments in their host (9, 10). In general, Complex II consists of four subunits (11). A flavoprotein subunit (SDH1, Fp) and an iron-sulfur subunit (SDH2, Ip) form a soluble heterodimer, which then binds to a membrane anchor heterodimer, SDH3 (CybL) and SDH4 (CybS). SDH1 contains a covalently bound FAD and catalyzes the oxidation of succinate to fumarate. SDH2 transfers electrons to ubiquinone via the [2Fe-2S] cluster in the N-terminal plant-type ferredoxin domain (Ip_N) and the [4Fe-4S] and [3Fe-4S] clusters in the C-terminal bacterial ferredoxin domain (Ip_C). Ubiquinone is bound and reduced in a pocket provided by SDH2, SDH3, and SDH4 (12–14). SDH3 and SDH4 contain three transmembrane helices and coordinate protoheme IX via histidine in the second helices of each subunit (11–14).

* This work was supported in part by Grant-in-aid for Scientific Research 20570124 (to T. M.), Creative Scientific Research Grant 18GS0314 (to K. K.), Grant-in-aid for Scientific Research on Priority Areas 18073004 (to K. K.) from the Japanese Society for the Promotion of Science, and Targeted Proteins Research Program (to K. K.) from the Japanese Ministry of Education, Science, Culture, Sports and Technology (MEXT). The costs of publication of this article were defrayed in part by the payment of page charges. This article must therefore be hereby marked "*advertisement*" in accordance with 18 U.S.C. Section 1734 solely to indicate this fact.

[S] The on-line version of this article (available at http://www.jbc.org) contains supplemental Table S1.

[1] Supported by a Japanese Government scholarship from Ministry of Education, Science, Culture, Sports and Technology.

[2] To whom correspondence may be addressed. Tel.: 81-3-5841-3526; Fax: 81-3-5841-3444; E-mail: tmogi@m.u-tokyo.ac.jp.

[3] Present address: Dept. of Microbiology, School of Life Dentistry at Tokyo, Nippon Dental University, Tokyo 102-8159, Japan.

[4] To whom correspondence may be addressed. Tel.: 81-3-5841-3526; Fax: 81-3-5841-3444; E-mail: kitak@m.u-tokyo.ac.jp.

[5] The abbreviations used are: SQR, succinate:quinone reductase; hrCNE, high resolution clear native electrophoresis; IC_{50}, the 50% inhibitory concentration; Ip_N, the N-terminal plant-type ferredoxin domain; Ip_C, the C-terminal bacterial ferredoxin domain; DCIP, 2,4-dichlorophenolindophenol; SML, sucrose monolaurate; Tricine, *N*-[2-hydroxy-1,1-bis(hydroxymethyl)ethyl]-glycine; MOPS, 3-(*N*-morpholino)propanesulfonic acid; Q_n, ubiquinone-*n*.

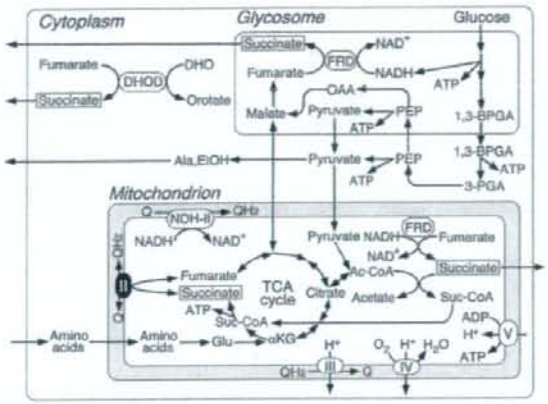

FIGURE 1. **Metabolic pathways in *T. cruzi*.** Incomplete oxidation of glucose takes place in glycosomes and mitochondria, and end products such as succinate, L-alanine, ethanol, and acetate are excreted from parasites (3, 4). Cytoplasmic dihydroorotate (*DHO*):fumarate reductase (*DHOD*) contributes succinate production (6).

Parasitic nematodes adapted to hypoxic host environments often have modified respiratory chains. Many adult parasites perform fumarate respiration by expressing a stage-specific isoform of Complex II (9, 10). *Hemonchus contortus* uses an isoform for SDH2 (9), whereas *Ascaris suum* uses isoforms for SDH1 and SDH4 (10). To explore the adaptive strategy in a parasitic protist, we isolated mitochondria from axenic culture of *T. cruzi* epimastigotes and characterized the purified Complex II. Our results demonstrated for the first time that *T. cruzi* Complex II is an unusual supramolecular complex with a heterodimeric iron-sulfur subunit and seven novel noncatalytic subunits. Purified enzyme showed reduced binding affinities for both substrates and inhibitors. Because this novel structural organization is conserved in all trypanosomatids (2, 15, 16), parasite Complex II would be a potential target for the development of new chemotherapeutic agents for trypanosomiasis and leishmaniasis.

EXPERIMENTAL PROCEDURES

Preparation of Mitochondria—*T. cruzi* strain Tulahuhen was grown statically for 6–7 days at 26 °C in 300-cm^2 cell culture flasks (Falcon, BD Biosciences) containing 250 ml of the modified LIT medium (17), supplemented with 0.1% (w/v) glucose, 0.001% (w/v) hemin (Sigma), and 5% (v/v) fetal bovine serum (MP Biochemicals). Mitochondria were isolated from epimastigotes by the differential centrifugation method (18) with slight modifications. Parasites grown to $6-8 \times 10^7$ cells/ml were washed with buffer A (20 mM Tris-HCl, pH 7.2, 10 mM NaH_2PO_4, 1 mM sodium EDTA, 1 mM dithiothreitol, 0.225 M sucrose, 20 mM KCl, and 5 mM $MgCl_2$). Cells were disrupted by grinding with silicon carbide (Carborundum 440 mesh; Nacalai Tesque, Kyoto, Japan) in the presence of a minimum volume of buffer B (25 mM Tris-HCl, pH 7.6, 1 mM dithiothreitol, 1 mM sodium EDTA, 0.25 M sucrose, and EDTA-free Complete protease inhibitor mixture (Roche Applied Science)). The resultant cell paste was resuspended in buffer B and centrifuged at 500 × *g* for 5 min and 1000 × *g* for 15 min to remove silicon carbide and nuclear fraction, respectively. The mitochondrial fraction was recovered upon centrifugation of the last supernatant at 10,000 × *g* for 15 min, washed three times in buffer B, and resuspended to a protein concentration of ~30 mg/ml and kept at −80 °C until use.

TABLE 1
Purification of complex II from *T. cruzi* mitochondria

Step	Protein	Succinate:DCIP reductase	Yield	Purification
	mg	*units*	*units/mg*	%	*-fold*
Mitochondria	314	27	0.085	100	1.0
SML extract	141	22	0.16	83	1.9
Source 15Q	7.8	7.6	0.97	28	12
Superdex 200 (1st)	1.3	1.4	1.09	5.3	13
Superdex 200 (2nd)	0.15	0.43	2.87	1.6	34

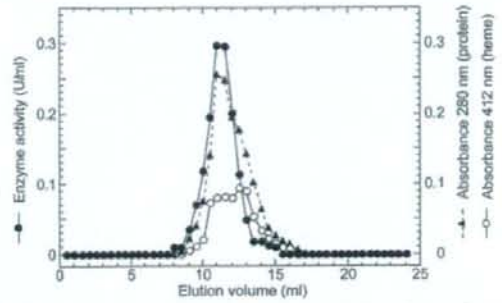

FIGURE 2. **Elution profile of *T. cruzi* Complex II on Superdex 200 chromatography.** Complex II fractions from the first gel filtration chromatography with a Superdex 200-pg column were concentrated and rechromatographed at the flow rate of 0.25 ml/min. Aliquots were collected every 0.5 ml. Elution profiles for proteins and cytochromes were monitored at 280 (▲) and 412 nm (○), respectively, and the enzyme activity (●) was measured as decylquinone-mediated succinate:DCIP reductase.

Isolation of Complex II—All steps were carried out at 4 °C. Mitochondrial fraction (~300 mg of protein from 10 liters culture) was brought to 70 ml with buffer C (10 mM KP_i, pH 7.5), 1 mM sodium EDTA, 1 mM sodium malonate, EDTA-free Complete protease inhibitor mixture (Roche Applied Science) (2 tablets/50 ml), 1% (w/v) sucrose monolaurate SM-1200 (SML) (Mitsubishi-Kagaku Foods Co., Tokyo, Japan)). The mixture was stirred for 30 min and centrifuged at 200,000 × *g* for 1 h. The supernatant was loaded at 1 ml/min onto a Source 15 Q column (1.6 inner diameter × 10 cm; GE Healthcare), equilibrated with buffer C containing 0.1% SML. After washing with 5 volumes of the same buffer, proteins were eluted with a 200-ml linear gradient of NaCl from 0 to 150 mM at 2 ml/min. Active fractions were concentrated to ~250 μl by ultrafiltration with Amicon Ultra-4 (molecular weight cutoff 100,000, Millipore) and subjected to gel filtration FPLC with a Superdex 200-pg 10/300 GL column (1 cm inner diameter × 30 cm; GE Healthcare) at 0.25 ml/min in 20 mM MOPS-NaOH, pH 7.2, containing 1 mM sodium EDTA, 1 mM sodium malonate, 150 mM NaCl, and 0.1% SML. Peak fractions were rechromatographed as above, and purified enzyme was concentrated and stored at −80 °C until use.

Identification of Complex II Subunits—The purified enzyme was subjected to 12.5% SDS-PAGE, and subunits were transferred to an Immobilon-P membrane (Millipore), followed by

staining with Coomassie Brilliant Blue R-250 (19, 20). Five or ten N-terminal amino acid residues were determined with a Procise 494 HT (Applied Biosystems) or an Hp G1005A (Hewlett-Packard Co.) Protein Sequencing System at the Bio-Medical Research Center of Juntendo University or APRO Life Science Institute, Inc. (Tokushima, Japan). When the N terminus was blocked, protein bands were digested with trypsin, and internal peptide sequences were determined (20). Genes coded for Complex II subunits were identified with BLASTP in the *T. cruzi* genome data base (15).

Phase Partitioning of Mitochondrial Fraction with Triton X-114—Phase partitioning by Triton X-114 was performed as described previously (21) with a slight modification. A total of 2–3 mg of mitochondrial fraction was resuspended in 1 ml of Tris-HCl, pH 7.5, 150 mM NaCl, 1 mM EDTA, 2 mM sodium malonate, Complete protease inhibitors mixture (Roche Applied Science) (2 tablets/50 ml), protease inhibitors mixture for mammalian cell and tissue extracts (Sigma) (10 μl/ml), and 2% (v/v) Triton X-114. The mixture was incubated for 30 min on ice and kept at −30 °C overnight. After thawing, the insoluble material was removed by centrifugation at 4 °C, and the supernatant was incubated for 10 min at 37 °C and centrifuged at 2000 × *g* for 10 min to separate the aqueous and detergent-rich phases. The aqueous phase was brought to 2% (v/v) Triton X-114, whereas the detergent-rich fraction was brought to 1 ml with the above buffer. After incubation on ice for 10 min, samples were incubated at 37 °C for 10 min and phases separated as before. This wash step was repeated three times. Finally, the samples were dialyzed and concentrated by Amicon Ultra-4 (Millipore) in the presence of 50 mM imidazole, 50 mM NaCl, 6 mM aminocaproic acid, 0.05% (w/v) deoxycholate, and 0.1% (w/v) SML, pH 7, and kept at −80 °C until use.

Enzyme Assay—Decylubiquinone-mediated succinate-2,4 dichlorophenolindophenol (DCIP) reductase activity was measured at 25 °C in 100 mM potassium phosphate, pH 7.4, containing 1 mM $MgCl_2$, 2 mM KCN, 0.1 mM antimycin A (Sigma), and 0.1% SML with 63 μM decylubiquinone (Sigma) *plus* 60 μM DCIP. After 2 min of incubation, reduction of DCIP (ϵ_{600} = 21 mM^{-1} cm^{-1}) was measured in the presence of 10 mM succinate. SQR activity was determined with 40 μM ubiquinone-2 (Q_2) (Sigma, ϵ_{278} = 12.3 mM^{-1} cm^{-1}). Kinetic analysis was done with KaleidaGraph version 4.0 (Synergy Software).

Miscellaneous—High resolution clear native electrophoresis (hrCNE) (22) was performed with 4–16% Novex gels (Invitrogen) using 0.02% dodecylmaltoside and 0.05% sodium deoxycholate for the cathode buffer additives, and the Complex II band was visualized by the activity staining (23) or Coomassie Brilliant Blue. Tricine-PAGE analysis was done with Novex 10–20% Tricine gels (Invitrogen), and proteins bands were sequentially stained by Sypro ruby (Invitrogen) and silver. During purification the succinate-decylubiquinone-DCIP reduc-

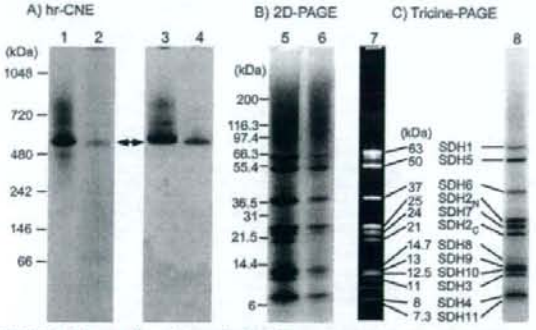

FIGURE 3. **Electrophoresis analysis of *T. cruzi* Complex II.** *A*, purified Complex II (2 μg; *lanes 1* and *3*) and the detergent-rich fraction from the phase partitioning by Triton X-114 of the mitochondrial fraction (60 μg; *lines 2* and *4*) were subjected to hrCNE. Proteins were stained by Coomassie Brilliant Blue (*left panel*), and Complex II was visualized by SDH activity staining (*right panel*). *B*, proteins of Complex II showing SDH activity in *A* were analyzed by 10–20% Tricine SDS-PAGE and visualized by silver stain (*lane 5*, pure complex; *lane 6*, detergent-rich fraction). *C* shows the subunit composition of the pure Complex II from *T. cruzi* stained by SYPRO ruby (*lane 7*) or silver stain (*lane 8*). Molecular weight standards used are NativeMark (Invitrogen, *lane 1*) and Mark 12 unstained standards (Invitrogen, *lanes 5* and *7*).

TABLE 2
Identification of genes encoding subunits for *T. cruzi* complex II

Subunit[a]	Sequence confirmed[b]	Accession number or RefSeq ID at NCBI (haplotype,[c] M_r)	Identity[d]	TM[e]
			%	
SDH1	Ser^{10}–Met^{19}	AB031741 (NE, 66,974), XP_809281 (E, 18,231)	59	0
SDH5	Ala^{10}–Leu^{19}	XP_818124 (NE, 53,831), XP_810172 (E, 20,788)	16	0
$SDH2_N$	Ser^{188}–Arg^{196}, Lys^{201}–Ile^{204}, Gly^{221}–Asn^{223}, Glu^{267}–Ile^{268}	XP_814994 (merged, 32,232)[f]	24 (37)	0
$SDH2_C$	Pro^{2}–Leu^{6}	XP_803796 (NE, 21,352), XP_806126 (E, 21,379)	25 (43)	0
SDH6a	Val^{19}–Val^{28}	XP_809065 (NA, 36,077), XP_812789 (NA, 36,035)	15	0
SDH6b	Val^{19}–Val^{28}	XP_813603 (NA, 36,133), XP_813645 (NA, 36,039)	14	0
SDH7	Ile^{26}–Leu^{35}	XP_813318 (NE, 28,218), XP_820239 (E, 28,202)	22	0
SDH3	Val^{2}–Phe^{11}	XP_809410 (NE, 12,176), XP_810064 (E, 12,204)	29	1
SDH4	Phe^{39}–Thr^{48}	XP_808211 (E, 13,957), XP_816430 (NE, 13,975)	27	2
SDH8	Gly^{5}–Met^{16}	XP_809192 (NE, 16,199), XP_817545 (E, 16,143)	ND[g]	2
SDH9	Ile^{10}–Pro^{19}	XP_807105 (merged, 15,736)	ND	1
SDH10	Pro^{25}–Val^{33}	XP_808894 (NE, 15,565), XP_808903 (E, 15,554)	ND	1
SDH11	Phe^{20}–Cys^{29}	XP_814088 (E, 10,346), XP_814509 (NE, 10,337)	ND	1

[a] Alleles were named as SDH3-1 (XP_809410) and SDH3-2 (XP_810064) in the order of the accession numbers, except for SDH5.
[b] These are *N*-terminal sequences except for $SDH2_N$ and SDH8, where the N-terminal residues were blocked.
[c] Homozygous alleles located in a merged assembly of Esmeraldo (E) and non-Esmeraldo (NE) homologous sequences whose different copies were merged genes during the genome assembly are indicated by "merged." Haplotypes for gene with more than two copies in the genome that does not belong to a merged region are not assigned (NA).
[d] Identity % to counterparts in human were as follows: SDH1 (D30648), SDH2 (P21912), SDH3 (Q99643), or SDH4 (O14521). In parentheses, the identity % of $SDH2_N$ and $SDH2_C$ that correspond to either Met^{1}–Pro^{155} (Ip_N domain) or Tyr^{156}–Val^{280} (Ip_C domain), respectively, of human SDH2 is shown. Identity % for truncated forms of SDH1 and SDH5 (SDH1-2 and SDH5-2) in the Esmeraldo haplotype was 66 and 20%, respectively.
[e] Transmembrane segments (TM) were estimated with TMHMM (52) and SOSUI (53).
[f] SDH2N from other trypanosomatids lack Met^{1} to Arg^{42} of $TcSDH2_N$.
[g] ND indicates not determined because these hydrophobic sequences are a highly divergent form of mammalian sequences.

12-Subunit Complex II from T. cruzi

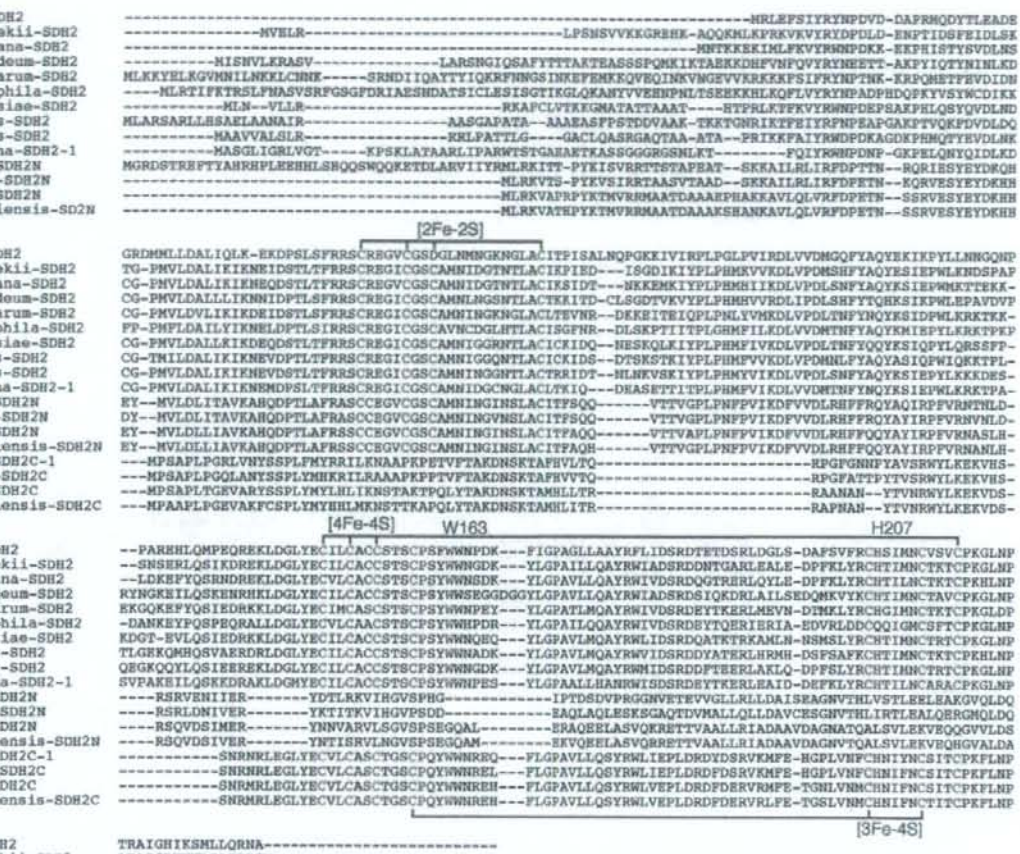

FIGURE 4. **Alignment of heterodimeric SDH2 sequences.** Amino acid residues proposed for binding of the iron-sulfur clusters are shown in *red* and those for the quinone binding in *blue*. Residue numbers refer to the *E. coli* SDH2 (SdhB) sequence. GenBank™ accession numbers for $SDH2_N$ and $SDH2_C$ sequences used are *T. cruzi* (XP_814994 and XP_803796), *T. brucei* (XP_847169 and XP_826981), and *L. major* (XP_001683488 and XP_001682013). Other SDH2 sequences used are *E. coli* (NP_415252), *Rickettsia prowazekii* (Q9ZEA1), *Reclinomonas americana* (NP_044798), *Dictyostelium discoideum* (XP_646559), *Plasmodium falciparum* (D86574), *Tetrahymena thermophila* (XP_001024894), *S. cerevisiae* (NP_012774), *Caenorhabditis elegans* (NP_495992), *H. sapiens* (NP_002991), and *A. thaliana* (NP_189374).

tase activity was monitored in a microplate spectrophotometer (Benchmark Plus, Bio-Rad). Kinetics and UV-visible absorption spectra were determined at room temperature with a V-660 UV-visible spectrophotometer (Jasco, Tokyo, Japan). Protoheme IX and protein concentrations were determined by pyridine hemochromogen method (24) and the micro BCA method (Pierce), respectively. Sequence alignment was done with ClustalX 2.0 (25).

RESULTS AND DISCUSSION

Isolation of T. cruzi Complex II—To determine the molecular organization of *T. cruzi* Complex II, we purified this enzyme from epimastigote mitochondria by ion-exchange and gel filtration chromatography using the nonionic detergent sucrose monolaurate (Table 1). Decylubiquinone-mediated succinate: DCIP reductase activity was eluted as a single peak at each step

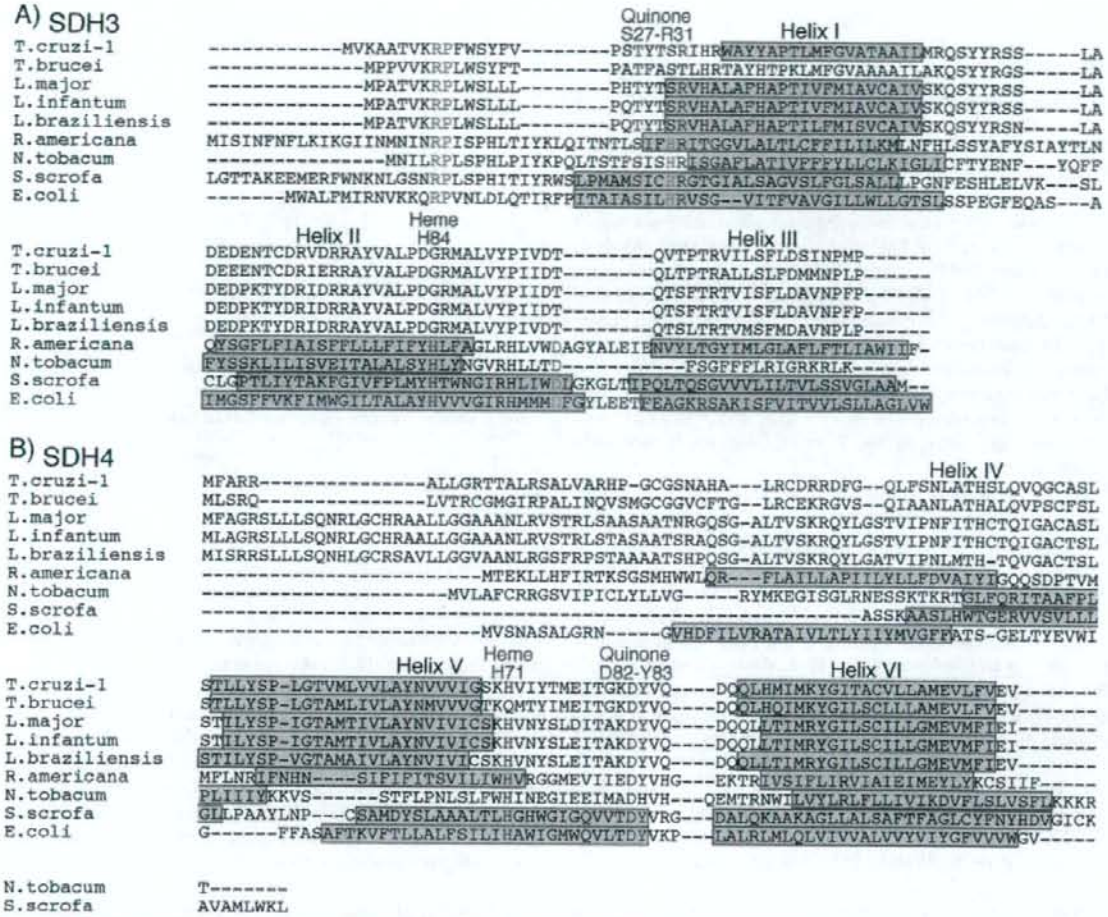

FIGURE 5. **Alignments of SDH3 (*A*) and SDH4 (*B*) sequences.** Amino acid residues proposed for binding of protoheme IX are shown in *red* and those for the quinone binding in *blue*. Other conserved residues are indicated by *green*. Transmembrane helices found in *E. coli* (Protein Data Bank code 1NEK) and porcine (Protein Data Bank code 1ZOY) Complex II are shown by *red rectangles*, and transmembrane helices predicted by TMHMM are indicated by *blue rectangles*. TMHMM failed to predict transmembrane helices in *T. brucei* SDH3. Residue numbers refer to *E. coli* SDH3 (SdhC) and SDH4 (SdhD). GenBank™ accession numbers for SDH3 and SDH4 sequences used are *T. cruzi* (XP_809410, XP_808211), *T. brucei* (XP_845531, XP_823384), *L. major* (XP_001684890, XP_001685874), *L. infantum* (XP_001467132), *L. braziliensis* (XP_001566908, XP_001567905), *R. americana* (NP_044796, NP_044797), *Nicotiana tobacum* (YP_173376, YP_173457), *Sus scrofa* (1ZOY_C, 1ZOY_D), and *E. coli* (NP_415249, NP_415250).

and co-eluted with proteins and *b*-type cytochrome(s) at the second Superdex 200 chromatography (Fig. 2). Specific activity was increased 34-fold to 2.9 units/mg proteins, and the yield was ~2%. A hrCNE of the pure protein identified *T. cruzi* Complex II as an ~550-kDa complex (Fig. 3, *lanes 1* and *3*), which is 4-fold larger than bovine and yeast Complex II (130 kDa) and potato Complex II (150 kDa) (26, 27). Upon phase partitioning of the mitochondrial fraction with Triton X-114, the Complex II of *T. cruzi* was found only in the detergent-rich fraction (data not shown). Analysis of the detergent-rich fraction by hrCNE showed the Complex II as a single band at the same position as the pure enzyme (~550 kDa) (Fig. 3, *lanes 2* and *4*). These results indicated that the purified Complex II was obtained in its intact form. Interestingly, second dimensional analysis of both the purified Complex II and the detergent-rich fraction from phase partitioning with Triton X-114 with SDH activity showed that *T. cruzi* Complex II is composed of 12 subunits (Fig. 3, *lanes 5* and *6*). The same subunit composition was obtained by immunoaffinity purification of the partially purified enzyme (data not shown). The apparent molecular weight of the subunits ranges from 7.3 to 63 kDa (Fig. 3, *lanes 7* and *8*). Assuming the presence of equimolar amounts of subunits, a total molecular mass of Complex II would be 286.5 kDa, indicating that *T. cruzi* Complex II is a homodimer.

Identification of Genes Coded for Subunits—We determined N-terminal sequences (or internal peptide sequences in case of $SDH2_N$ and SDH8) of all subunits and identified genes coded for SDH1-1, $SDH2_N$, $SDH2_C$, SDH5–SDH7 (hydrophilic sub-

units), SDH3, SDH4, and SDH8–SDH11 (hydrophobic subunits) (Table 2). All subunits, except SDH1-1, are trypanosomatid-specific and structurally unrelated to plant-specific soluble subunits (AtSDH5–AtSDH8, 5–18 kDa) (27–29). All genes (except SDH6 with four copies) are present as two copies, which are assigned to either Esmeraldo or non-Esmeraldo haplotype (haploid genotype) in *T. cruzi* subgroup IIe. In contrast, only one copy each of the orthologues is present in *T. brucei*, *Leishmania major*, *Leishmania infantum*, and *Leishmania braziliensis* (supplemental Table S1). N-terminal sequence analysis of SDH3 and SDH7 showed that yields of two isoforms are similar (*i.e.* SDH3-1:SDH3-2 = 63:37, and SDH7-1:SDH7-2 = 54:46), indicating that isoforms are expressed from each haplotype. Because truncated isoforms for SDH1 and SDH5 in the Esmeraldo haplotype (see below) are not assembled into the 12-subunit complex and $SDH2_N$ and SDH9 isoforms have the identical sequence, 512 ($= 1^4 \times 4^1 \times 2^{(12-5)}$) kinds of heterogeneity may exist in the *T. cruzi* Complex II monomer (Table 2).

Flavoprotein Subunit—SDH1-1 (63-kDa band in Tricine-PAGE) cross-reacted with the antiserum against bovine SDH1 (data not shown) and is highly homologous to counterparts in *T. brucei* (93% identity), *L. major* (90%), *Homo sapiens* (59%), *Arabidopsis thaliana* (62%), *Saccharomyces cerevisiae* (61%), and *Escherichia coli* (48%, SdhA). Amino acid residues proposed for dicarboxylate binding and a FAD ligand histidine (12–14) are all conserved in SDH1-1. SDH1-1 and SDH5-1 of the non-Esmeraldo haplotype share a weak sequence similarity in the entire region, but the latter lacks amino acid residues responsible for FAD and dicarboxylate binding. In the Esmeraldo haplotype, SDH1-2 and SDH5-2 are truncated and contain only Met^1 to Gly^{167} of TcSDH1-1 and Ile^{305} to Met^{486} of TcSDH5-1, respectively (Table 2). These findings suggest that TcSDH1-1, TcSDH1-2, TcSDH5-1, and TcSDH5-2 might have evolved by gene duplication and subsequent degeneration.

Iron-Sulfur Subunit—Sequence analysis of the 25- and 21-kDa band proteins revealed that they contain the plant ferredoxin domain (Ip_N) and bacterial ferredoxin domain (Ip_C) of canonical SDH2 (Ip) in the N- and C-terminal half, respectively (Fig. 4). Sequence identities of Ip_N and Ip_C are 37 and 43%, respectively, to those of human SDH2 (Table 2), and the Ip_N and Ip_C domains contain all amino acid residues responsible for binding of iron-sulfur clusters and ubiquinone (12, 13, 30) (Fig. 4). Such a heterodimeric Ip subunit can be found in *T. brucei* (31), *T. cruzi*, *L. major*, *L. infantum*, and *L. braziliensis* (Tables 2), which belong to the order Trypanosomatida. Thus we named these subunits as $SDH2_N$ and $SDH2_C$, respectively.

Splitting of mitochondrial membrane proteins has been reported for cytochrome *c* oxidase CoxII in Apicomplexa and Chlorophyceae (32, 33), and ATP synthase α subunit in *Leishmania tarentolae* and *T. brucei* (34, 35). The former occurs at the gene level and the latter by post-translational cleavage. Sequence analysis indicates that heterodimeric SDH2 and CoxII have emerged from gene duplication followed by degeneration of the N- or C-terminal half of the duplication products. Conserved domains in degenerated duplicons, which have arisen from mitochondrion-to-nucleus transfer of the duplicated genes (32, 33, 36), must retain the potential for protein-protein interactions and constitute a heterodimeric functional subunit by trans-complementation.

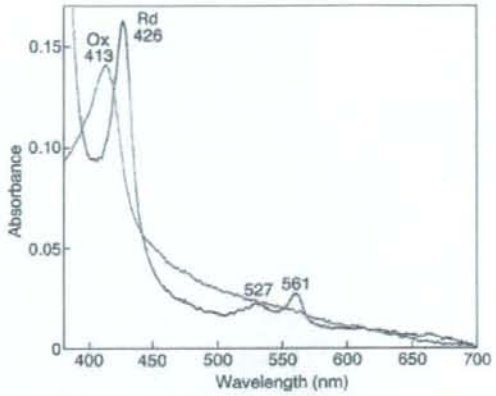

FIGURE 6. **Visible absorption spectra of *T. cruzi* Complex II.** Purified Complex II was desalted by ultrafiltration and diluted with 0.1 M sodium phosphate, pH 7.2, containing 0.1% SML at a final concentration of 0.06 mg/ml. Absorption spectra of the air-oxidized (*Ox, thin line*) and dithionite-reduced (*Rd, thick line*) forms were recorded at room temperature with UV-2400 spectrophotometer (Shimadzu Corp., Kyoto, Japan).

Membrane Anchor Subunits—Membrane anchor subunits in protist enzymes are highly divergent from bacterial and mammalian counterparts and difficult to find with conventional BLAST programs. We identified candidates for *T. cruzi* SDH3 and SDH4 by the presence of the quinone/heme-binding motifs "$RPX_{16}SX_2HR$ (SDH3 helix I)" and "$HX_{10}DY$ (SDH4 helix V)," respectively, present in membrane anchor subunits. In Complex II, Trp^{164} in SDH2 (Fig. 4) and Tyr^{83} in the SDH4 $HX_{10}DY$ motif (Fig. 5*B*) (*E. coli* numbering) could hydrogen bond to the O-1 atom of ubiquinone and contribute to the binding affinity (12, 37). Arg^{31} in the SDH3 SX_3HR motif (Fig. 5*A*) and Asp^{82} in the SDH4 $HX_{10}DY$ motif are in close proximity to ubiquinone and could interact with Tyr^{83} (37). Ser^{27} in the SDH3 SX_2HR motif has been shown to be essential for quinone binding (38) and is a candidate for hydrogen bonding to the O-4 atom of ubiquinone (30). The first arginine (Arg^9 in *E. coli* SDH3) in the $RPX_{16}SX_3R$ motif is in the vicinity of Glu^{186} in SDH1 and Asp^{106} in SDH2 and may play a structural role by making a hydrogen bond network.

In *T. cruzi*, SDH3 has the "$RPX_{11}SX_2HR$ motif in front of the predicted transmembrane helix I and lacks transmembrane helices II and III. However, sequence alignment suggests the presence of the alternative motif "$TX_2SR/(T)$" in the Trypanosomatida (Fig. 5*A*). In mitochondrial Complex II, protoheme IX is ligated by two His residues in the second transmembrane helix of SDH3 ("$HX_{10}D$" motif) and SDH4 ("$HX_{10}DY$" motif). A heme ligand in helix II (His^{84} in *E. coli* SDH3) may be substituted by a nearby histidine in the quinone-binding motif "SX_2HR" (39). In contrast, SDH4 lacks helix IV and appears to interact with heme and ubiquinone with the $HX_{10}DY$ motif. As in rice SDH4 (GenBank™ accession number NP_001045324), the heme ligand His is substituted by Gln in *T. brucei* SDH4. The presence of a bound heme or an alternative ligand in *T.*